Oxidation and fractional crystallization in olivine from chondrule-composition melts

Will Vaughan

May 31, 2011

[Topazos] accidit in Arabiae insula, quae Cytis vocabatur, in quam devenerant Trogodytae praedones fame et tempestate fessi, ut, cum herbas radicesque foderent, eruerent topazon.

Olivine occurs on an island in the Red Sea called Cytis [Zabargad]. A group of pirates who were exhausted from a storm landed on this island; starving, they dug for herbs and roots, but found olivine instead.

Pliny the Elder

Abstract

In order to explain the conflicting Ti valence and fayalite (Fa) content of olivine in Semarkona (LL3) chondrules, chondrule-composition melts were reduced at log f_{O2} = IW−3.0 and cooled under more oxidizing conditions (IW−0.5). The resulting run products present another problem: what information about the extent and timescale of oxidation of metallic iron during olivine crystallization is recorded by the Fa profiles of olivine crystals, which have cores as low as Fa_9 and rims as high as Fa_{50}? Fractional crystallization is modeled with the Rayleigh equation. Measured Ca and Cr profiles are used to determine the extent of crystallization of olivine and to predict the concentration of Fe; Fe concentrations higher than those predicted by this model are attributed to progressive oxidation of metallic iron. The results suggest that over 90% of Fa variation is due to oxidation and that most oxidation of metallic iron happens in less than an hour. This oxidation timescale is for a total gas pressure of 1 bar and so is not applicable to the solar nebula, where the gas pressure is orders of magnitude smaller.

Contents

1 Introduction **7**

2 Samples and methods **8**
2.1 Sample preparation 8
2.2 Sample analysis 9

3 Results **10**
3.1 New Concord 10
3.2 Isothermal runs 12
3.3 Cooling runs 15

4 Discussion **22**
4.1 The importance of oxidation 22
4.2 The rate and extent of oxidation 23

5 Conclusions **32**

A Appendices **33**
A.1 Rayleigh fractionation and two derivations of the Rayleigh equation . . . 33
A.2 Derivation and calculation of uncertainties in concentrations measured by electron microprobe 35

List of Figures

1 Fayalite content and titanium valence across olivine in a Semarkona type II chondrule. Figure reproduced from Simon (2011). 7
2 BSE image showing major minerals and texture of New Concord. Ol – olivine; Pyx – pyroxene; Og – oligoclase feldspar; Fe – iron-nickel metal; FeS – troilite; AVs – alteration veins. 10
3 BSE image showing metamorphosed New Concord barred olivine chondrule. Oligoclase feldspar (Og) fills the interstices between parallel bars of olivine (Ol) and pyroxene (Pyx). Metallic iron (Fe) is present outside the chondrule at lower left. 11
4 BSE image showing major minerals and texture of two isothermal runs, 10-1 (soaked for 23.75 hours) and 09-5 (soaked for 165 hours). Ol – forsteritic olivine; Pyx – enstatitic pyroxene; Fe – iron-nickel metal; Gl – glass. . . . 12
5 Crystal size distributions for 10-1 (soaked for 23.75 hours) and 09-5 (soaked for 165 hours). The radius used is that of a circle with the same area as the crystal in section. 13
6 Reduction of New Concord starting material and evidence of disequilibrium in isothermal runs. New Concord olivine and pyroxene averages are plotted on this graph at 0 hours of soak time. Error bars correspond to plus/minus one standard deviation. 15

7 BSE image showing major minerals and texture of two cooling runs: CR3 (cooled to 1192°C) and CR5 (cooled to 800 °C). Ol – forsteritic olivine; Pyx – enstatitic pyroxene; Fe – iron-nickel metal; Gl – glass. 15
8 Oxidation of iron metal: isothermal run 10-1 and cooling runs CR4, CR1, and CR5 ordered by decreasing quench temperature. 17
9 Chemistry of glass in the isothermal and cooling runs. 10-1 glass composition is plotted on this graph at 1400°C. Error bars correspond to plus/minus one standard deviation. 18
10 Mole percent fayalite across cooling run olivines. . . . 19
11 Crystal size distributions for the cooling runs. The radius used is that of a circle with the same area as the crystal in section. 20
12 BSE image showing major minerals and texture of CR11 (cooled to 715°C at log f_{O_2} = IW−3.0). Ol – forsteritic olivine; Pyx – enstatitic pyroxene; Fe – iron-nickel metal; Gl – glass. 21
13 Mole percent fayalite across olivine from CR11 (cooled to 715°C at log f_{O_2} = IW−3.0). 22
14 Fractional crystallization model fit to the Ca profile from a CR4 olivine grain and applied to predict Cr and Fe in that grain. 1σ Ca = 0.01 weight percent, 1σ Cr = 0.02 weight percent, and 1σ Fe = 0.1 weight percent (Appendix B). 26
15 Fractional crystallization model fit to the Ca profile from a CR5 olivine grain and applied to predict Cr and Fe in that grain. 1σ Ca = 0.01 weight percent, 1σ Cr = 0.02 weight percent, and 1σ Fe = 0.1 weight percent (Appendix B). 27
16 Fractional crystallization model fit to the Ca profile from a CR11 olivine grain and applied to predict Cr and Fe in that grain. 1σ Ca = 0.01 weight percent, 1σ Cr = 0.02 weight percent, and 1σ Fe = 0.1 weight percent (Appendix B). 29
17 Linear and logarithmic models for C_{sol0} as a function of R applied to predict Fe in a CR4 olivine grain. a, k, and initial C_{sol0} are the same as in Figure 14. 1σ Fe = 0.1 weight percent (Appendix B). 30
18 Models stepping C_{sol0} to predict Fe in CR4 and CR5 olivine grains. Predicted curves are labeled with their corresponding C_{sol0} (weight percent Fe). 1σ Fe = 0.1 weight percent (Appendix B). 31

List of Tables

1 Bulk composition of New Concord (Jarosewich 1990) and type II Semarkona chondrule average (Jones 1994). The total for New Concord includes several components that are not reported in this table. 8
2 Run conditions for five isothermal runs (ordered by increasing soak time) and seven cooling runs (prefixed with CR, ordered by decreasing quench temperature). 9
3 Modal abundances in New Concord and the total area measured. 10

4 Compositional homogeneity in New Concord minerals. Averages and standard deviations are based on 6 measurements of separate mineral grains for olivine, 3 measurements for pyroxene, and 5 measurements for oligoclase. 12
5 Modal abundances in 10-1 (soaked for 23.75 hours) and 09-5 (soaked for 165 hours) and the total area measured. 13
6 Compositional homogeneity within and across five isothermal runs in order of increasing soak time. Averages and standard deviations are based on more than five measurements of separate mineral grains or interstices of glass, except for 09-5 (averages and standard deviations for olivine and pyroxene are based on 2 measurements; averages for glass are based on 1 measurement) and in 10-1 (in which there is only one olivine analysis). 14
7 Modal abundances in cooling run products (ordered by decreasing quench temperature) and the total area measured. Abundances from three separate chips of CR3 and the average CR3 abundances weighted by area are also reported. 16
8 Glass compositions in all six cooling runs and pyroxene compositions in runs CR6 and CR5. Runs are ordered by decreasing quench temperature. All averages and standard deviations are based on more than five measurements of separate pyroxene grains or interstices of glass. 18
9 Pyroxene and glass composition for CR11 (cooled to 715°C at log f_{O_2} = IW$-$3.0). All averages and standard deviations are based on more than five measurements of separate pyroxene grains or interstices of glass. . . 21
10 Distribution coefficients measured from glass and olivine crystals in the isothermal runs compared to published distribution coefficients at 1200°C with 100°C/hour cooling at log f_{O_2} = IW$-$0.5 (Kennedy et al. 1993). 26
11 Peak and background intensities (counts/second) and count times (seconds) for Ca, Cr, and Fe measured on standards and on a representative olivine grain from CR1 plus calculated σ_k/K. 35

1 Introduction

The fayalite content and titanium valence of olivine in chondrules from the unmetamorphosed Semarkona meteorite (LL3) give contradictory information about the oxygen fugacity (f_{O_2}) of the environment in the solar nebula where these chondrules formed (Simon et al. 2008). Figure 1 shows that nearly one-fifth of the total titanium in olivine from a Semarkona type II chondrule (a chondrule in which molar Fe/(Fe+Mg) > 0.1) is trivalent. The fayalite content of olivine in this chondrule ($X_{Fa} > 0.15$) implies a log $f_{O_2} \geq$ IW$-$1.8 (Ebel and Grossman 2000); however, the ratio of trivalent titanium to total titanium is not much smaller than that measured in pyroxene from a charge equilibrated at a log f_{O_2} of IW$-$6.8 (Beckett 1986; Grossman et al. 2008).

There are several possible explanations for the discordance between these oxybarometers. One is kinetic: trivalent titanium might be left over from a reduced precursor and oxidize more slowly than iron. Other explanations are thermodynamic: trivalent titanium might exist at equilibrium in olivine at higher oxygen fugacities than in pyroxene, or trivalent titanium might exist over a wide range of oxygen fugacities in both olivine and pyroxene. In order to determine which explanation is correct, John Beckett (Caltech) melted and held chondrule-composition powders of New Concord (L6) in a reducing gas (log f_{O_2} = IW$-$3.0) and cooled them in a more oxidizing gas (IW$-$0.5). The compositions and titanium valences of olivine, pyroxene, and glass in the run products were measured by electron microprobe and x-ray absorption near-edge spectroscopy (XANES). The results, reported by Simon et al. (2011), do not rule out the thermodynamic or kinetic explanations above: they show that trivalent titanium can persist from a reduced precursor, but also that a substantial fraction of total titanium may exist as trivalent titanium in olivine and pyroxene over a wide range of oxygen fugacities.

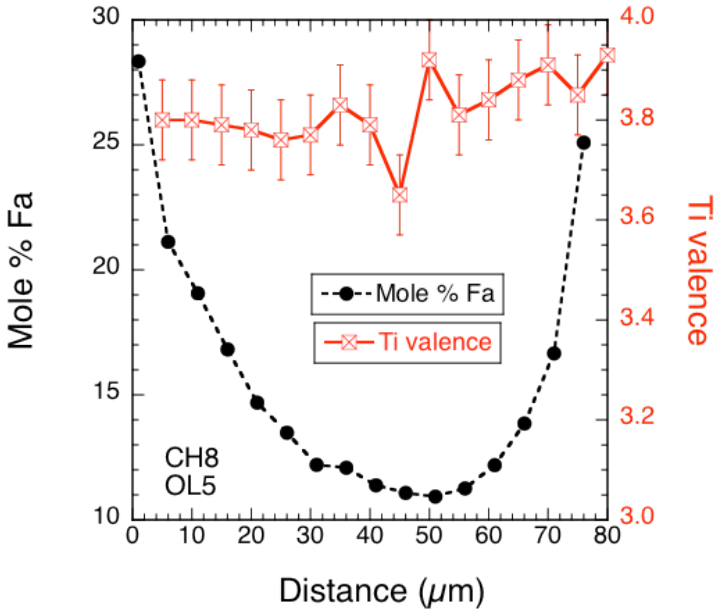

Figure 1: Fayalite content and titanium valence across olivine in a Semarkona type II chondrule. Figure reproduced from Simon (2011).

Olivine crystals from these chondrule-composition melt experiments are strongly zoned, with a large internal range of fayalite content: olivine grains from runs cooled at IW-0.5 have Fa_{10} cores and Fa_{40-50} rims. It is not clear if oxidation of metallic iron must be invoked to explain this fayalite variation, or whether fractional crystallization of a starting liquid, given the slight incompatibility of Fe^{2+} in olivine at the temperatures and oxygen fugacities of these experiments (Kennedy et al. 1993), is sufficient to explain the fayalite range observed. Further experiments performing oxidation without cooling or cooling without oxidation would untangle the contributions that oxidation and fractional crystallization make to the fayalite range observed in these samples. An experiment performing cooling without oxidation is described in the Results.

Ignoring the possibility of further experiments, it would be interesting to determine from these samples alone the relative contributions of oxidation and fractional crystallization to the fayalite content of the olivine grains and to determine the timescale and extent of oxidation. It might even be useful–a method for determining the importance, timescale, and extent of oxidation proved on these samples could be adapted to interpret the oxidation history of olivine in natural chondrules (the olivine in the Semarkona chondrule shown in Figure 1, for instance). This thesis reports the petrography and mineral chemistry of the New Concord starting material and twelve run products; models the contributions of oxidation and fractional crystallization to the fayalite profiles of olivine grains in these run products; demonstrates the importance of oxidation in producing the high fayalite contents observed in these grains; and constrains the timescale and extent of oxidation of metallic iron.

2 Samples and methods

2.1 Sample preparation

Twelve of the thirteen samples described in this thesis were prepared by John Beckett at Caltech. A powder of New Concord was used as an analog for a type II chondrule composition (see Table 1). The powder was melted on iron loops in a gas-mixing furnace held at a temperature of 1400°C and at an oxygen fugacity of log f_{O_2} = IW-3.0. Oxygen fugacity for the isothermal runs and for the cooling runs described below was buffered by a H_2-CO_2 gas at a pressure of 1 atm. This period of isothermal reduction will hereafter be referred to as the soak. Five run products were soaked for periods from 24 to 165 hours and quenched in order to characterize the mineral assemblage at 1400°C and IW-3.0, as well as to judge the time necessary for devolatilization and crystal-liquid equilibration. These five constant-temperature runs are called isothermal runs.

	SiO_2	TiO_2	Al_2O_3	Cr_2O_3	FeO	MnO	MgO	CaO	Na_2O	K_2O	P_2O_5	FeS	FeNi (m)	Total
New Concord	39.90	0.13	2.24	0.52	14.68	0.33	24.65	1.68	1.04	0.11	0.18	5.84	8.23	99.56
Type II Semarkona	45.1	0.10	2.68	0.51	14.9	0.39	31.3	1.89	1.65	0.17	0.34	0.94	0.51	100.38

Table 1: Bulk composition of New Concord (Jarosewich 1990) and type II Semarkona chondrule average (Jones 1994). The total for New Concord includes several components that are not reported in this table.

In ten runs, starting material was soaked for 15-20.5 hours, cooled at a constant rate (ranging from 10°C/hour to 1000°C/hour) while exposed to a gas with log f_{O_2} = IW−0.5, and quenched at temperatures ranging from 1296°C to 709°C. In an additional run, starting material soaked for 17 hours was cooled at 100°C/hour to 715°C at log f_{O_2} = IW−3.0. These eleven decreasing-temperature runs are referred to as cooling runs. Out of these eleven cooling runs, only the seven that cooled at 100°C/hour are considered in this thesis. Table 2 lists the run conditions for all twelve run products considered.

Sample.	Soak temp. (°C)	Soak time (hr)	Soak f_{O_2}	Cooling f_{O_2}	Cooling rate (°C/hr)	Quench temp. (°C)
10-1	1400	23.75	IW−3	NA	NA	NA
09-1	1400	42.5	IW−3	NA	NA	NA
09-4	1400	69	IW−3	NA	NA	NA
09-3	1400	99	IW−3	NA	NA	NA
09-5	1400	165	IW−3	NA	NA	NA
CR4	1400	15	IW−3	IW−0.5	100	1296
CR3	1400	16	IW−3	IW−0.5	100	1192
CR7	1400	20.5	IW−3	IW−0.5	100	1101
CR1	1400	15.5	IW−3	IW−0.5	100	1000
CR6	1400	15	IW−3	IW−0.5	100	896
CR5	1400	17.5	IW−3	IW−0.5	100	800
CR11	1400	17	IW−3	IW−3	100	715

Table 2: Run conditions for five isothermal runs (ordered by increasing soak time) and seven cooling runs (prefixed with CR, ordered by decreasing quench temperature).

2.2 Sample analysis

The twelve run products described in Table 2 and a thick section of New Concord were analyzed at the University of Chicago. The quenched run products arrived as hollow, glassy, gray-colored spheres about half a centimeter wide. The spheres were broken into fragments, mounted in epoxy on glass slides, and ground flat and polished. A JEOL 5800-LV scanning electron microscope was used with a 15 kv, 1.5 nA beam to take secondary electron (SE) and backscattered electron (BSE) images of sample surfaces. Images were combined into photomosaics to show larger areas of section surface using Adobe Photoshop CS4's Photomerge utility. Modal abundances of minerals and glass were measured using ImageJ software (Abramoff et al. 2004). Chemical compositions of minerals and glass were measured using a Cameca SX50 electron microprobe in wavelength-dispersive mode with a 15 kV, 15 nA focused beam less than 1 micron in diameter. Composition data were processed in Microsoft Excel and visualized using gnuplot software (Williams and Kelley 2010).

3 Results

3.1 New Concord

New Concord is composed of five major minerals: in order of decreasing modal abundance, these are olivine, pyroxene, oligoclase feldspar, iron-nickel metal, and troilite. Figure 2 shows these minerals and Table 3 gives their modal abundances. Olivine, pyroxene, and feldspar occur in two different textures. In the first texture, illustrated in Figure 3, olivine and pyroxene occur in long bars or radial spikes generally several hundred microns long and less than fifty microns wide. Grain boundaries are often marked by fractures; feldspar is present in these breaks between bars. There are no large agglomerations, and very few smaller blebs, of metal or sulfide. This texture occurs inside elliptical areas around half a millimeter in diameter. The second texture, illustrated in Figure 2, is more nearly equigranular. Olivine and pyroxene grains are equant and usually between 50 to 200 microns in size. Feldspar fills the interstices between grains and also forms larger crystals, some up to a hundred microns in size. Metal and sulfides are present in large agglomerations on the order of 100 microns in size and rarely as smaller blebs.

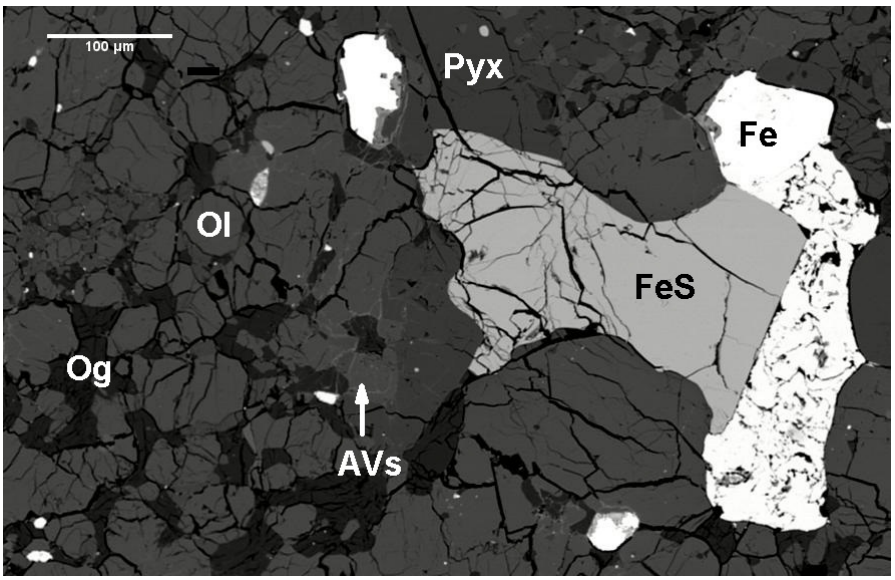

Figure 2: BSE image showing major minerals and texture of New Concord. Ol – olivine; Pyx – pyroxene; Og – oligoclase feldspar; Fe – iron-nickel metal; FeS – troilite; AVs – alteration veins.

FeS	Fe	Og	Pyx	Ol	Area (mm^2)
1.5	5.3	17.6	33.2	42.4	36.7

Table 3: Modal abundances in New Concord and the total area measured.

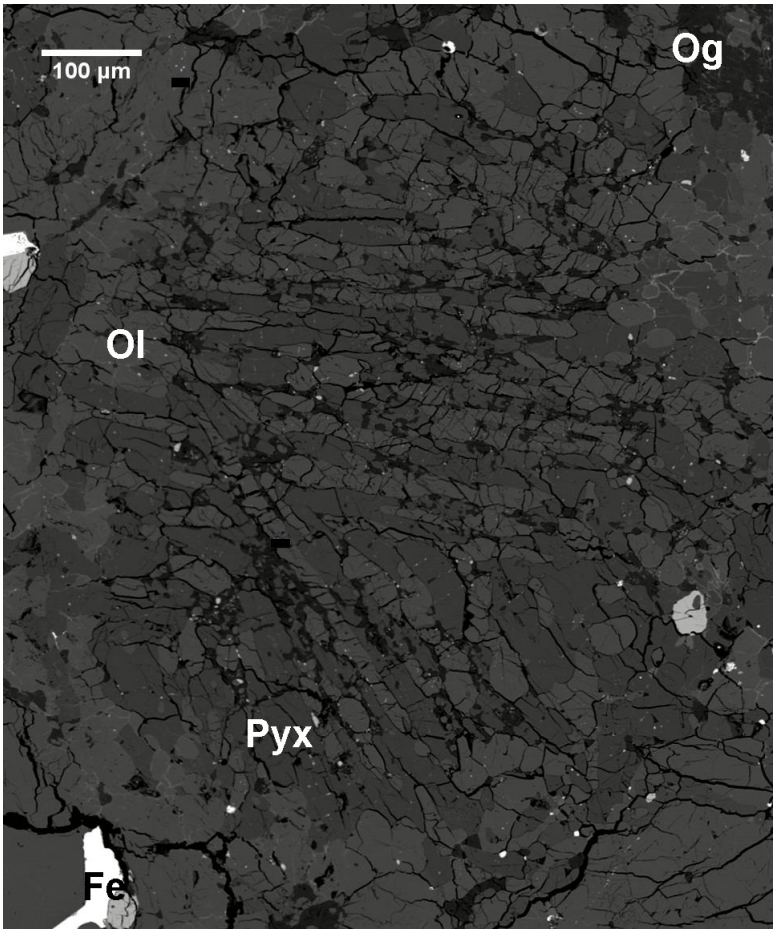

Figure 3: BSE image showing metamorphosed New Concord barred olivine chondrule. Oligoclase feldspar (Og) fills the interstices between parallel bars of olivine (Ol) and pyroxene (Pyx). Metallic iron (Fe) is present outside the chondrule at lower left.

New Concord is an L6 chondrite; i.e., it is interpreted as having been extensively metamorphosed by heating: the first texture described above is produced from the metamorphism of barred or radial olivine chondrules, and the second texture is produced from the metamorphism of matrix. In both textures, but particularly the metamorphosed matrix, there are accessory grains of chromite, as well as alteration veins containing a phase with relatively high average atomic number, probably pyrrhotite (Lee and Bland 2004).

Mineral grains in New Concord are compositionally homogeneous. BSE images do not show evidence of zoning in olivine or pyroxene, as evidenced by the even brightness of grains in Figures 2 and 3. The small standard deviations in weight percent of major oxides, particularly FeO and MgO (both less than 0.5 in pyroxene and olivine), from microprobe analyses of thirteen mineral grains (Table 4) also indicate compositional homogeneity. The average olivine composition is Fo_{75}, the average pyroxene composition is $En_{78}Fs_{21}$, and the average feldspar composition is $Ab_{77}An_{17}Or_6$ (oligoclase).

	SiO_2	TiO_2	Al_2O_3	Cr_2O_3	FeO	MnO	MgO	CaO	Na_2O	K_2O	Total
Ol average	37.72	0.02	0.02	0.02	22.52	0.41	38.13	0.02	0.01	0.00	98.87
Ol std. dev.	0.43	0.01	0.02	0.02	0.33	0.07	0.44	0.01	0.01	0.00	0.72
Pyx average	55.01	0.17	0.15	0.12	13.65	0.43	28.67	0.87	0.01	0.01	99.09
Pyx std. dev.	0.19	0.01	0.02	0.02	0.21	0.05	0.21	0.06	0.01	0.01	0.48
Og average	66.52	0.05	22.47	0.00	0.66	0.01	0.02	2.16	6.48	0.66	99.01
Og std. dev.	1.71	0.01	0.44	0.00	0.07	0.01	0.04	0.03	3.27	0.14	1.33

Table 4: Compositional homogeneity in New Concord minerals. Averages and standard deviations are based on 6 measurements of separate mineral grains for olivine, 3 measurements for pyroxene, and 5 measurements for oligoclase.

3.2 Isothermal runs

All five isothermal runs are mineralogically and texturally similar and are considered together. The mineral assemblage of the isothermal runs is different from that of New Concord: the runs contain, in order of decreasing modal abundance, olivine and pyroxene, glass (quenched liquid), and iron-nickel metal. Figure 4 shows these minerals. There is no feldspar, troilite, or pyrrhotite in any of the isothermal runs because heating devolatilizes Na and S. Modal abundances are given in Table 5 for 10-1, the isothermal run soaked for the shortest time (24 hours), and 09-5, the run soaked for the longest time (165 hours); intermediate isothermal runs were only mapped with SE images, which do not have sufficient average atomic number contrast to distinguish olivine, pyroxene, and glass. In fact, olivine and pyroxene have such a similar average atomic number in these isothermal runs that they are indistinguishable by brightness in a BSE image (accordingly, olivine and pyroxene are grouped in Table 5). The modal abundance of metal changes by nearly twenty percent with an additional 141.25 hours of soaking, showing that a 23.75 hour soak is not long enough to reach equilibrium modal abundances. It is long enough to alter the New Concord mineral assemblage, however: the isothermal run 10-1 is about 14% metallic iron by volume, whereas New Concord is only 5% metallic iron by volume.

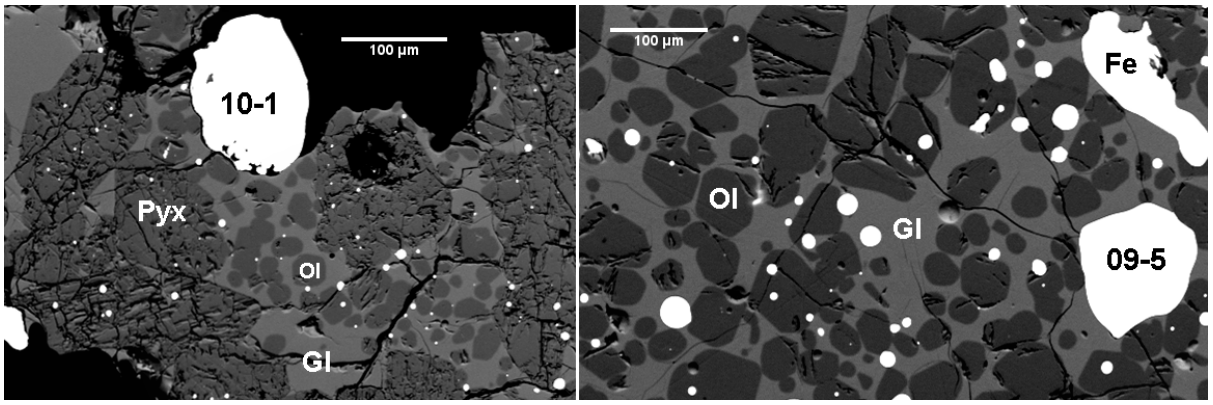

Figure 4: BSE image showing major minerals and texture of two isothermal runs, 10-1 (soaked for 23.75 hours) and 09-5 (soaked for 165 hours). Ol – forsteritic olivine; Pyx – enstatitic pyroxene; Fe – iron-nickel metal; Gl – glass.

	Fe	Glass	Ol + Pyx	Area (mm^2)
10-1	13.7	30.5	55.7	0.81
09-5	11.7	31.8	56.5	1.61

Table 5: Modal abundances in 10-1 (soaked for 23.75 hours) and 09-5 (soaked for 165 hours) and the total area measured.

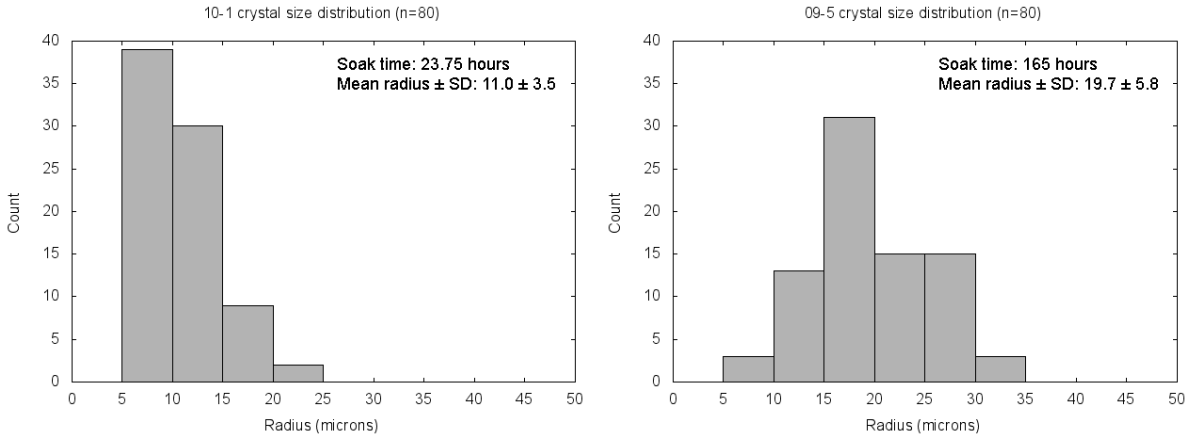

Figure 5: Crystal size distributions for 10-1 (soaked for 23.75 hours) and 09-5 (soaked for 165 hours). The radius used is that of a circle with the same area as the crystal in section.

Although olivine and pyroxene have the same BSE brightness, they are distinguishable by their cleavage: all pyroxene grains have well-developed, right-angle cleavage, but olivine grains have no cleavage. From this fact and two BSE photomosaics it can be determined that, although the volume percent of olivine plus pyroxene increases by only 1% between 10-1 and 9-5, the ratio of olivine to pyroxene changes substantially: 10-1 has much more pyroxene than olivine and 09-5 has much more olivine than pyroxene. Also, olivine crystals grow from an average radius of 11 microns in 10-1 to an average radius of 20 microns in 09-5 (Figure 5). Total SiO_2 should be the same in both runs, but there is less iron metal (and accordingly more FeO) in 09-5; therefore, as observed, 09-5 should contain more olivine, which has a higher (Fe+Mg)/Si ratio than pyroxene. Also, the distribution of olivine and pyroxene may be uneven within each run product: for example, in both charges pyroxene rings the surfaces of the hollow run product spheres, whereas olivine and glass fill the gaps between these pyroxene walls (see 10-1 in Figure 4): 09-5 has more interwall area, so perhaps the sample heterogeneity accounts for some of the olivine/pyroxene discrepancy.

Mineral grains within each isothermal run are compositionally homogeneous. BSE images show no evidence of zoning in olivine or pyroxene, as evidenced by the even brightness of grains in Figure 4. 95 microprobe analyses of separate mineral grains and pockets of glass from all five isothermal runs are presented in Table 6. Mineral and glass compositions are similar, but not the same, between runs: for example, the average FeO weight percent of olivine in 09-1 (1.62 ± 0.24) is different from the average FeO weight percent of olivine in 09-4 (2.13 ± 0.08) at the 1σ level. All other major

elements, however, are the same at the 1σ level in olivine, pyroxene, and glass. Olivine and pyroxene reach an average olivine composition of Fo_{98} and an average pyroxene composition of En_{97}. Figure 6, however, shows evidence of olivine and pyroxene disequilibrium: pyroxene in 10-1, soaked for only 23.75 hours, has an average FeO of 2.46 $\pm$ 0.49, 2σ above the average FeO of pyroxene in 09-1 (1.24 $\pm$ 0.15). The isothermal runs are devolatilized: New Concord has 1.04 weight percent Na_2O and 0.11 weight percent K_2O (Table 1), but even the glass in the resulting melt has only 0.01 weight percent Na_2O and K_2O.

		SiO_2	TiO_2	Al_2O_3	Cr_2O_3	FeO	MnO	MgO	CaO	Na_2O	K_2O	Total
10-1	Ol average	41.19	0.01	0.02	0.44	2.48	0.18	54.04	0.13	0.01	0.00	98.50
	Pyx average	57.88	0.04	0.24	0.58	2.46	0.40	37.90	0.26	0.01	0.01	99.78
	Pyx std. dev.	0.60	0.02	0.04	0.05	0.49	0.04	1.14	0.03	0.01	0.01	1.08
	Gl average	55.65	0.41	9.40	0.75	3.13	0.25	21.42	7.93	0.05	0.02	99.02
	Gl std. dev.	0.60	0.03	0.28	0.04	0.11	0.11	0.87	0.24	0.15	0.06	0.50
09-1	Ol average	42.52	0.02	0.03	0.33	1.62	0.06	55.93	0.16	0.01	0.00	100.68
	Ol std. dev.	0.34	0.02	0.01	0.03	0.24	0.03	0.30	0.01	0.01	0.00	0.34
	Pyx average	59.42	0.05	0.29	0.42	1.24	0.32	38.47	0.29	0.01	0.01	100.52
	Pyx std. dev.	0.21	0.03	0.03	0.07	0.15	0.18	0.14	0.02	0.01	0.01	0.17
	Gl average	55.87	0.44	9.70	0.52	2.14	0.04	21.91	8.54	0.02	0.01	99.19
	Gl std. dev.	0.50	0.03	0.21	0.03	0.24	0.03	0.34	0.10	0.01	0.01	0.12
09-4	Ol average	42.08	0.02	0.03	0.41	2.13	0.05	55.45	0.15	0.01	0.00	100.33
	Ol std. dev.	0.31	0.01	0.01	0.02	0.08	0.03	0.35	0.02	0.01	0.00	0.49
	Pyx average	59.17	0.06	0.32	0.48	1.36	0.27	38.59	0.28	0.01	0.01	100.55
	Pyx std. dev.	0.37	0.02	0.04	0.04	0.21	0.13	0.32	0.02	0.01	0.01	0.46
	Gl average	55.44	0.42	9.06	0.66	3.16	0.08	21.70	7.89	0.02	0.01	98.43
	Gl std. dev.	0.57	0.02	0.44	0.04	0.77	0.03	0.26	0.14	0.01	0.01	0.73
09-3	Ol average	41.76	0.01	0.03	0.34	2.41	0.04	55.21	0.16	0.01	0.00	99.97
	Ol std. dev.	0.25	0.02	0.01	0.03	0.19	0.02	0.22	0.01	0.00	0.01	0.52
	Pyx average	58.55	0.05	0.33	0.49	1.62	0.30	38.01	0.29	0.02	0.00	99.66
	Pyx std. dev.	0.30	0.02	0.04	0.06	0.40	0.11	0.43	0.02	0.01	0.01	0.27
	Gl average	55.28	0.43	9.40	0.52	3.22	0.06	21.59	7.93	0.02	0.01	98.45
	Gl std. dev.	0.57	0.02	0.52	0.04	0.59	0.03	0.20	0.10	0.01	0.01	0.55
09-5	Ol average	41.46	0.03	0.04	0.29	2.22	0.04	56.02	0.15	0.00	0.00	100.23
	Ol std. dev.	0.59	0.02	0.00	0.00	0.06	0.03	0.84	0.01	0.01	0.00	0.38
	Pyx average	58.63	0.04	0.28	0.50	1.85	0.38	38.27	0.29	0.01	0.00	100.25
	Pyx std. dev.	0.56	0.01	0.03	0.04	0.37	0.06	0.26	0.01	0.01	0.00	0.37
	Gl average	55.46	0.50	10.37	0.42	2.67	0.11	21.83	8.34	0.02	0.00	99.71

Table 6: Compositional homogeneity within and across five isothermal runs in order of increasing soak time. Averages and standard deviations are based on more than five measurements of separate mineral grains or interstices of glass, except for 09-5 (averages and standard deviations for olivine and pyroxene are based on 2 measurements; averages for glass are based on 1 measurement) and in 10-1 (in which there is only one olivine analysis).

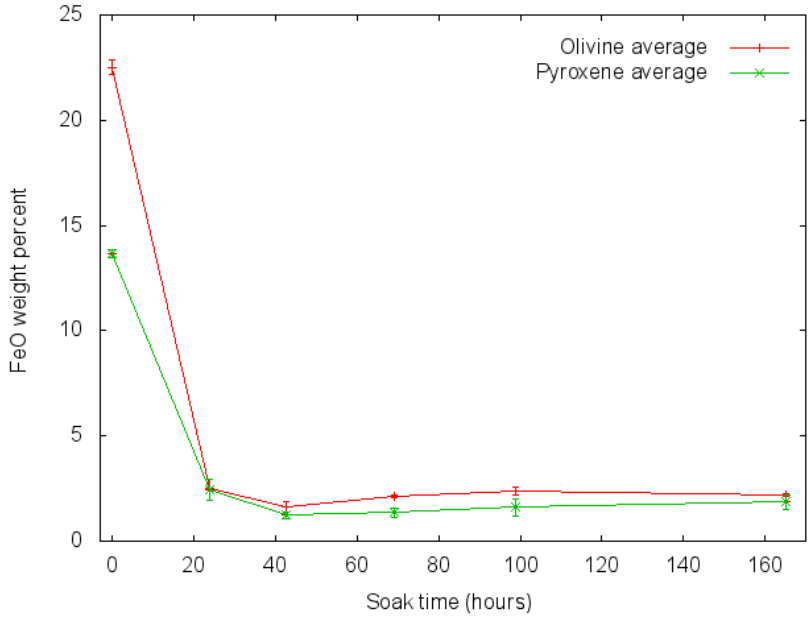

Figure 6: Reduction of New Concord starting material and evidence of disequilibrium in isothermal runs. New Concord olivine and pyroxene averages are plotted on this graph at 0 hours of soak time. Error bars correspond to plus/minus one standard deviation.

3.3 Cooling runs

The six cooling runs oxidized at log f_{O_2} = IW−0.5 are treated separately from CR11, the cooling run held at IW−3.0. These six cooling runs have the same mineral assemblage as, and textures similar to, the isothermal runs described above: all runs contain olivine, glass, and iron metal; CR6 and CR5, the cooling runs quenched at the lowest temperatures, also contain pyroxene. Figure 7 shows these minerals.

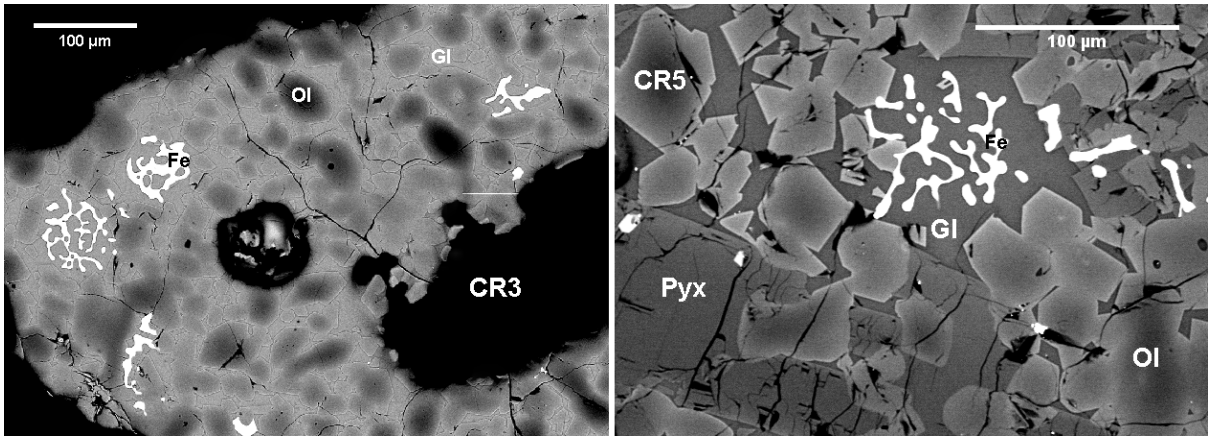

Figure 7: BSE image showing major minerals and texture of two cooling runs: CR3 (cooled to 1192°C) and CR5 (cooled to 800 °C). Ol – forsteritic olivine; Pyx – enstatitic pyroxene; Fe – iron-nickel metal; Gl – glass.

The modal mineralogy of these six cooling runs is reported in Table 7. The measured modal abundances should be treated with caution: the abundance of metallic iron varies by nearly 37% across three chips of the same run product, CR3. This variation can be attributed to sampling error: the run product chips are all less than half a centimeter in size, and metallic iron can be seen in the isothermal runs and in several of the cooling runs to occur in agglomerations hundreds of microns wide, so the percent area of metallic iron on a section surface may substantially misrepresent the percent volume of metallic iron in that run product. These spatial variations can also be explained by crystal settling: dense minerals may have sunk (and liquid may have risen) into different regions of the run product. For example, CR3 chip 4S might be a section near the bottom of a spherical run product, with high modal abundance of dense metallic iron and relatively dense olivine and low modal abundance of less dense glass. This would explain its small size relative to the other chips. CR3 chips 3 and 1S might be sections above the base of a run product, with less metallic iron and greater modal abundance of less dense glass.

	Fe	Glass	Ol + Pyx	Area (mm^2)
CR4	14.6	22.3	63.1	0.61
CR3 (chip 1S)	6.0	36.8	57.2	0.86
CR3 (chip 3)	17.9	33.8	48.3	0.84
CR3 (chip 4S)	42.6	23.4	33.5	0.34
CR3 (wt. avg.)	17.0	33.6	49.6	NA
CR7	1.9	35.6	62.5	1.36
CR1	9.1	24.9	66.0	0.34
CR6	1.1	36.8	62.5	0.36
CR5	6.6	34.1	59.3	0.29

Table 7: Modal abundances in cooling run products (ordered by decreasing quench temperature) and the total area measured. Abundances from three separate chips of CR3 and the average CR3 abundances weighted by area are also reported.

The modal abundances of the four cooling runs quenched at lower temperatures than CR3 are not nearly as variable as the modal abundances within that run product, varying only by 8.0% metallic iron and 5.7% olivine + pyroxene. Metallic iron has permanently decreased in abundance to somewhere between 1% to 9% in these runs from 14% in the isothermal runs and 14.6% in CR4 and 17% in CR3. It may decrease somewhat further from CR7 to CR5, but the cooling run modal abundance data are too noisy to tell. Metallic iron changes form between the isothermal runs and the cooling runs (Figure 8): in the isothermal runs, metal is present in the glass as convex blebs hundreds of microns across and as smaller, round blebs about ten microns in diameter. In the cooling runs, the large blebs have developed pockets and hollows and the smaller blebs have disappeared almost entirely.

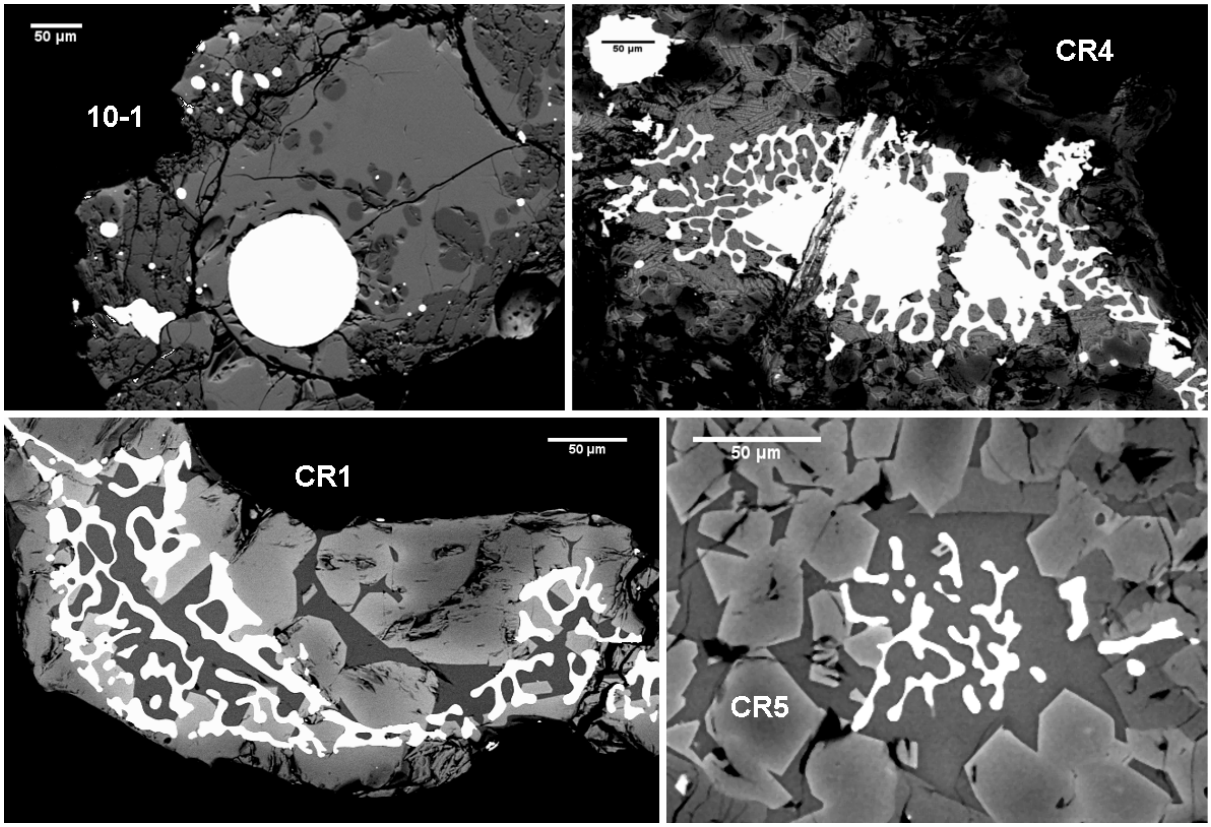

Figure 8: Oxidation of iron metal: isothermal run 10-1 and cooling runs CR4, CR1, and CR5 ordered by decreasing quench temperature.

The chemical composition of glass and pyroxene in the cooling runs is variable (Table 8). Weight percent FeO in the glass increases dramatically from 3.1% in the isothermal run 10-1 (Table 6) to 35.4% in CR4 due to the oxidation of iron metal. The increase in FeO dilutes the concentrations of the other oxides: weight percent SiO_2 and MgO in the glass decrease from 55.6% and 21.4%, respectively, in 10-1 to 38.2% and 5.0% in CR4. Despite this dilution, the concentrations of Al_2O_3 and CaO in the glass increase from 9.4% and 7.97% in 10-1 to 10.28% and 8.23% in CR4, probably because both Al and Ca are excluded from olivine. FeO starts to decrease and SiO_2 starts to increase in the cooling runs past CR4 due to olivine crystallization (olivine is poorer in SiO_2 than the liquid, so olivine crystallization causes an SiO_2 increase in the liquid). The slope of this increase and decrease decreases around 1100°C, perhaps due to slowing crystallization. The glass is chemically heterogeneous: in CR4, SiO_2 and FeO in glass, major elements that each make up more than 35 weight percent of glass on average, have standard deviations of 2.41 and 5.09 weight percent, respectively. Some heterogeneity is to be expected since metallic iron, the major driver of chemical changes in the liquid, is not evenly distributed; also, interstices of the liquid may be chemically isolated. Pyroxene is not present in runs CR4 through CR1, maybe because high FeO in the liquid promotes the crystallization of olivine, which has a higher (Fe+Mg)/Si ratio than pyroxene. Pyroxene appears by 896°C in CR6; it becomes 19 weight percent poorer in FeO (and richer in MgO) between CR6 and CR5.

		SiO_2	TiO_2	Al_2O_3	Cr_2O_3	FeO	MnO	MgO	CaO	Na_2O	K_2O	Total
CR4	Gl average	38.20	0.49	10.28	0.53	35.37	0.15	5.03	8.23	0.03	0.01	98.33
	Gl std. dev.	2.41	0.20	4.03	0.11	5.09	0.05	5.34	3.31	0.01	0.01	0.63
CR3	Gl average	40.69	0.63	13.29	0.18	26.19	0.11	7.43	9.97	0.04	0.01	98.54
	Gl std. dev.	0.88	0.10	0.23	0.02	0.40	0.01	2.20	1.17	0.01	0.01	0.31
CR7	Gl average	48.41	0.64	12.93	0.40	18.72	0.14	4.93	10.67	0.04	0.01	96.95
	Gl std. dev.	1.26	0.03	0.57	0.07	1.56	0.03	0.49	0.51	0.01	0.01	0.83
CR1	Gl average	50.99	0.70	15.21	0.15	16.86	0.14	2.50	11.35	0.17	0.01	98.10
	Gl std. dev.	1.59	0.08	1.10	0.05	1.19	0.04	0.21	0.69	0.02	0.01	0.29
CR6	Pyx average	49.19	0.24	3.23	1.42	22.43	0.23	18.16	3.39	0.00	0.01	98.33
	Pyx std. dev.	1.77	0.15	1.61	0.28	2.24	0.02	2.93	2.47	0.00	0.01	0.62
	Gl average	53.69	0.74	15.16	0.19	12.22	0.12	2.10	12.56	0.06	0.01	96.88
	Gl std. dev.	2.97	0.04	1.13	0.09	1.84	0.03	0.26	0.61	0.02	0.01	0.41
CR5	Pyx average	58.34	0.04	0.26	0.57	3.68	0.32	36.81	0.23	0.01	0.00	100.28
	Pyx std. dev.	0.71	0.02	0.05	0.05	2.12	0.08	1.46	0.03	0.01	0.00	0.57
	Gl average	55.28	0.72	15.80	0.17	11.09	0.12	2.46	12.50	0.10	0.01	98.30
	Gl std. dev.	2.00	0.05	2.21	0.08	1.57	0.03	0.26	0.53	0.02	0.01	0.57

Table 8: Glass compositions in all six cooling runs and pyroxene compositions in runs CR6 and CR5. Runs are ordered by decreasing quench temperature. All averages and standard deviations are based on more than five measurements of separate pyroxene grains or interstices of glass.

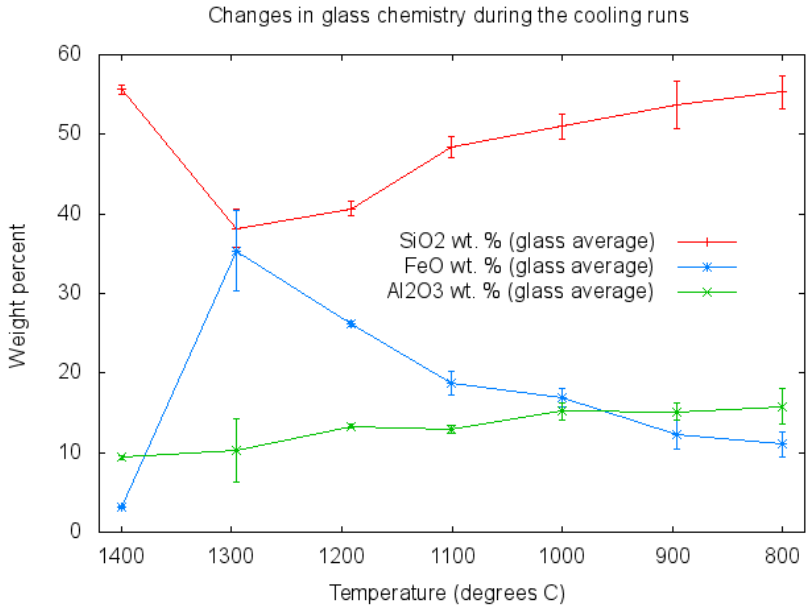

Figure 9: Chemistry of glass in the isothermal and cooling runs. 10-1 glass composition is plotted on this graph at 1400°C. Error bars correspond to plus/minus one standard deviation.

Olivine grains in the cooling runs are strongly zoned. Figure 10 shows fayalite profiles across several olivine grains from each run chosen for their low-Fa cores (which appear dark on a BSE image). These profiles have a range of nearly 45 mole percent fayalite: a grain from CR4 has a $Fa_{9.1}$ core, the lowest Fa measured in any cooling run olivine, and a $Fa_{45.5}$ rim; a rim from a CR1 olivine has $Fa_{53.9}$, the highest Fa measured. The profiles are roughly symmetric, with two arms of increasing fayalite content meeting at a low-Fa core. The isothermal run olivines are Fa_3; however, the cooling run olivines do not have cores more forsteritic than Fa_9. This could be caused by shorter soak times

for the cooling run olivines: the cooling runs were soaked for 15-20.5 hours, whereas the isothermal runs were soaked for $\geq$23.75 hours (Table 2). Crystal size distributions for olivine grains in the cooling runs (Figure 11) show a general increase in crystal size from 10-1 (Figure 5) to CR3 and from CR3 to CR4. There are almost no very small crystals: olivine crystallized around preexisting grains. The crystal size distributions for the four cooling runs with the lowest quench temperatures (CR7, CR1, CR6, and CR5) look very similar and have mean radii identical within 1σ, implying that crystallization slows by 1100°C.

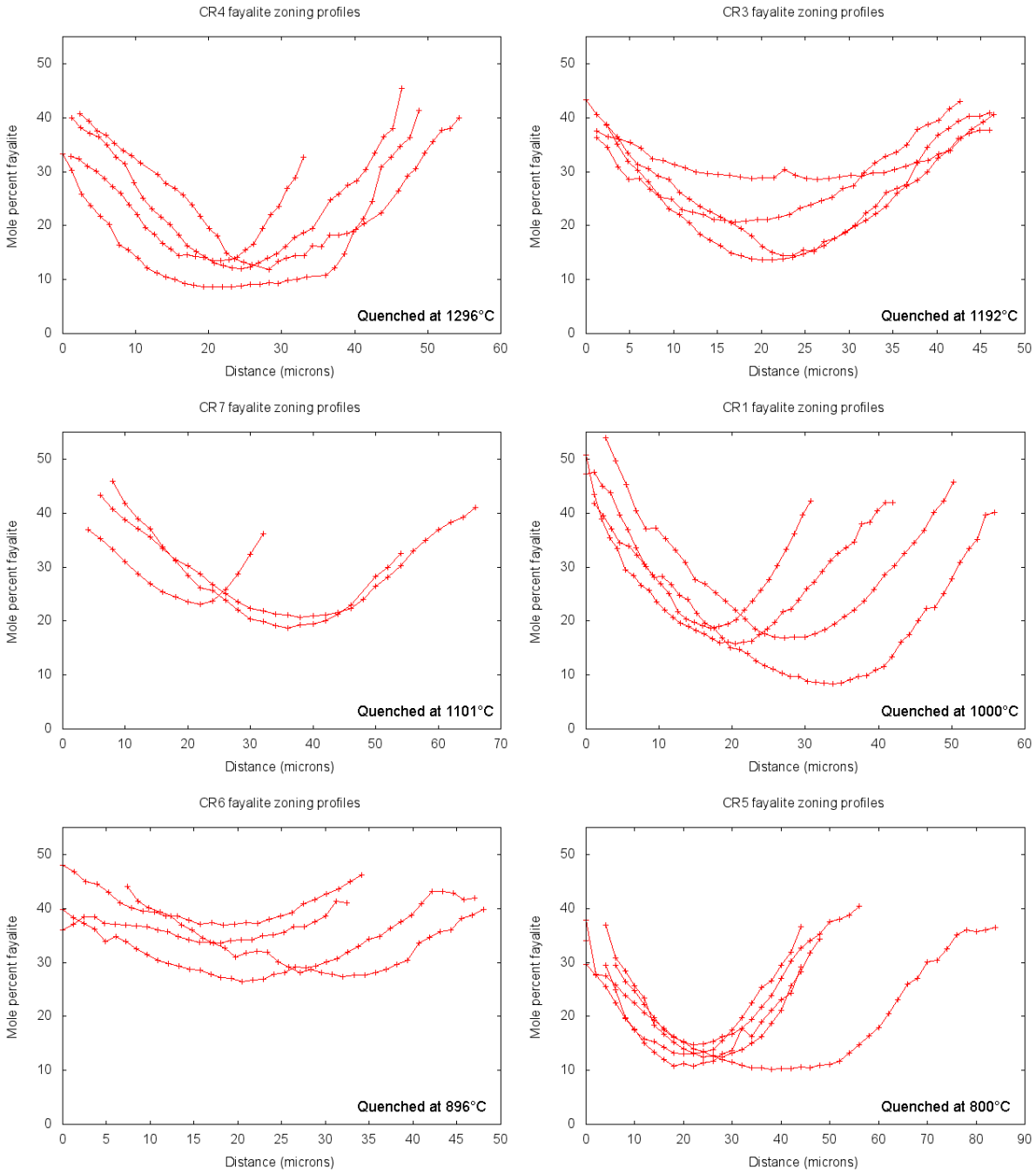

Figure 10: Mole percent fayalite across cooling run olivines.

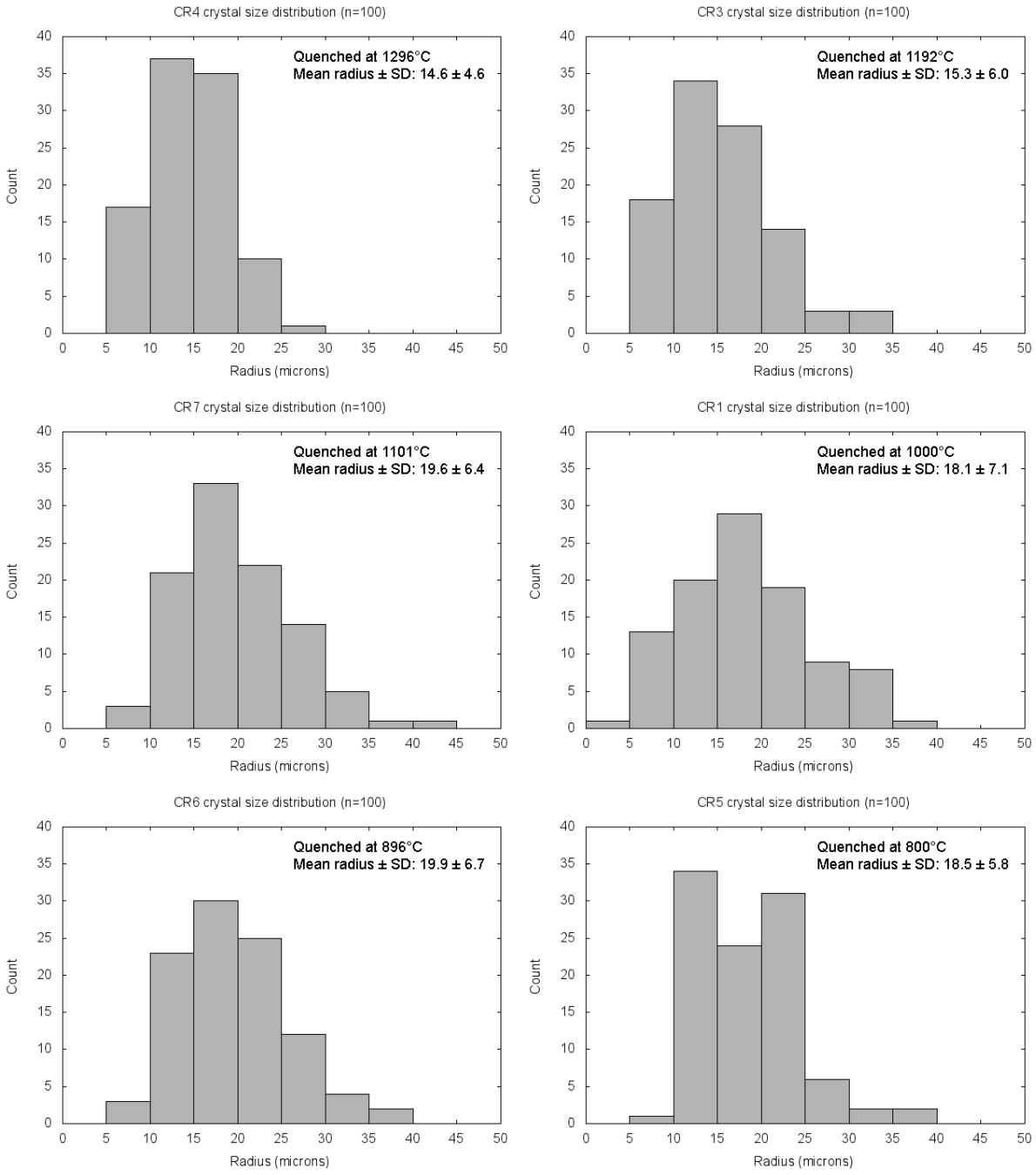

Figure 11: Crystal size distributions for the cooling runs. The radius used is that of a circle with the same area as the crystal in section.

CR11, which was cooled at 100°C/hr to 715°C at log f_{O_2} = IW−3.0, has different chemistry from the runs cooled at IW−0.5. Olivine grains show almost no zoning in a BSE image (Figure 12). Blebs of metallic iron are similar in shape to those from the isothermal runs. The average composition of four metal blebs from CR11 is $Fe_{94}Ni_3$; three metal blebs from the cooling run held at IW−0.5 for the longest time, CR5, have a higher average concentration of nickel, approximately $Fe_{60}Ni_{40}$. Figure 13 shows a fayalite profile across a CR11 olivine grain; this profile has a range of less than 1 mole percent fayalite (Fa_3 to $Fa_{3.9}$), only about 2% of the range seen in the cooling runs at log f_{O_2} = IW−0.5. Other grains show a similar Fa range. The glass chemistry (Table 9) is similar to the isothermal run: the average CR11 weight percent FeO and SiO_2 are 1.92% and 51.4%, similar to the values of 3.1 % and 55.6% measured in the isothermal run, although slightly less due to crystallization of olivine; FeO is thirteen times lower than in CR4. Pyroxene has only 2.73 weight percent FeO and is more magnesian than pyroxene in CR6 and CR5. There is not enough BSE imagery to measure modal abundances, but pyroxene is more abundant than olivine, reflecting a lower (Fe+Mg)/Si ratio than in the cooling runs. Clearly, cooling at IW−0.5 produces much more FeO-rich olivine, pyroxene, and glass than cooling at IW−3.0.

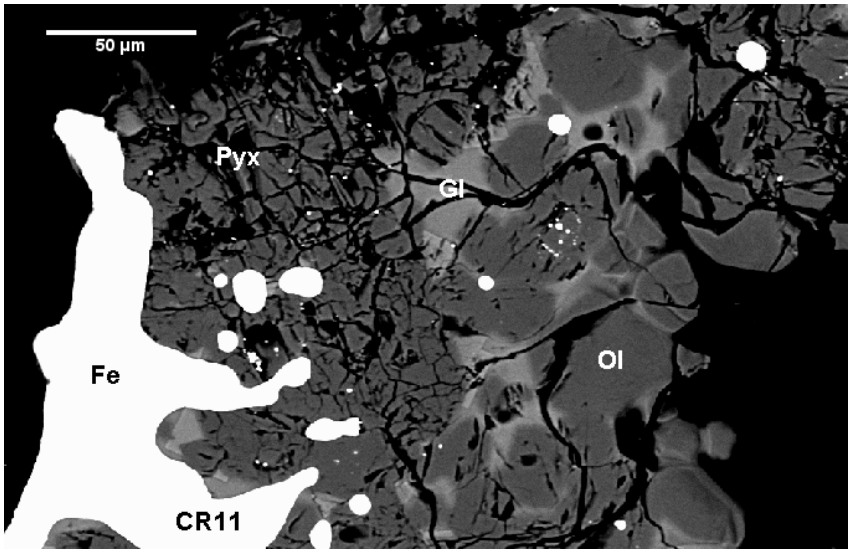

Figure 12: BSE image showing major minerals and texture of CR11 (cooled to 715°C at log f_{O_2} = IW−3.0). Ol – forsteritic olivine; Pyx – enstatitic pyroxene; Fe – iron-nickel metal; Gl – glass.

	SiO_2	TiO_2	Al_2O_3	Cr_2O_3	FeO	MnO	MgO	CaO	Na_2O	K_2O	Total
Pyx average	55.83	0.05	0.43	0.51	2.73	0.26	37.35	0.41	0.01	0.01	97.61
Pyx std. dev.	0.73	0.05	0.41	0.07	1.10	0.16	1.11	0.52	0.01	0.01	0.40
Gl average	51.40	0.48	21.45	0.18	1.92	0.09	6.47	13.24	0.06	0.02	95.31
Gl std. dev.	0.70	0.06	2.09	0.05	0.14	0.03	3.67	1.08	0.02	0.01	0.80

Table 9: Pyroxene and glass composition for CR11 (cooled to 715°C at log f_{O_2} = IW−3.0). All averages and standard deviations are based on more than five measurements of separate pyroxene grains or interstices of glass.

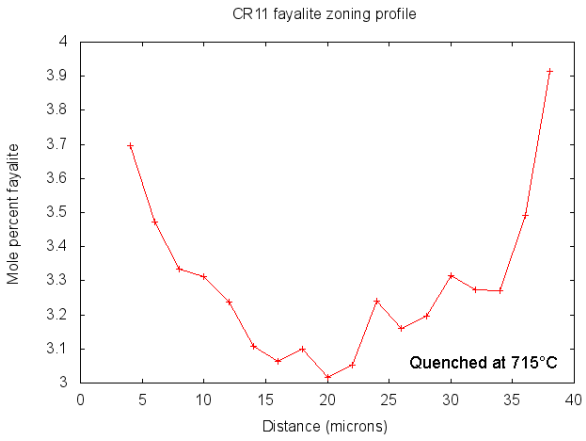

Figure 13: Mole percent fayalite across olivine from CR11 (cooled to 715°C at log f_{O_2} = IW−3.0).

4 Discussion

4.1 The importance of oxidation

The range of fayalite content in olivine grains from CR11, the run cooled to 715°C at log f_{O_2} = IW−3.0, shows that fractional crystallization of a liquid of composition similar to the glass from the isothermal run 10-1 produces only 2% of the fayalite range observed in olivine grains from the runs cooled at IW−0.5: compare Figure 11 to Figure 13. FeO must be added to the isothermal run liquid to produce the zoning profiles observed in the cooling runs at IW−0.5; Figure 9 shows that the glass from a run cooled at IW−0.5 to 1296°C has 32 weight percent more FeO than glass from the isothermal run 10-1.

This additional FeO comes from oxidation of metallic iron. There are three pieces of evidence suggesting that metallic iron is lost from the runs at IW−0.5: the decrease in the modal abundance of iron between 10-1 and the cooling runs, the change in the shape of metal grains from these runs, and the increase in Ni concentration from CR11 to CR5. Metallic iron decreases in abundance from 14% in the isothermal runs and 14.6% in CR4 or 17% in CR3 to somewhere between 1% to 9% in the cooling runs quenched at the lowest temperatures (Table 7). In the isothermal runs, metal is present in the glass as convex blebs hundreds of microns across and as many smaller blebs; in the cooling runs, the large blebs develop pockets and the smaller blebs have disappeared almost entirely (Figure 8). This change is due to the oxidation of metallic iron. The small blebs have been completely oxidized to FeO. The large blebs develop pockets since large-surface-area structures maximize the rate of oxidation. The average composition of the metal phase is approximately $Fe_{94}Ni_3$ in CR11 and $Fe_{60}Ni_{40}$ in CR5; assuming that CR11 has the same nickel concentration as the isothermal run 10-1, 95% of iron metal would have to have been lost during the time CR5 spent at IW−0.5. Metallic iron is lost from the runs at IW−0.5, but not from the runs at IW−3.0: the loss of metal must be due to oxidation at the higher f_{O_2}. In short, the oxidation of iron at log f_{O_2} = IW−0.5 provides the FeO that produces the fayalite range observed in these runs.

4.2 The rate and extent of oxidation

Oxidation contributed to the fayalite content observed in the cooling runs. It is not clear, however, on what time scale oxidation of metallic iron took place, or to what extent it progressed (beyond a few measurements of Ni concentration in the metal phase in CR11 and CR5). This section puts quantitative constraints on the rate and extent of oxidation by modeling fractional crystallization of Fe in olivine grains. Departures of the Fe profile calculated from a fractional crystallization model from a measured Fe profile are assumed to result from an increase in weight percent FeO in the liquid due to oxidation of metallic iron.

Fractional crystallization is described by the Rayleigh equation (Appendix A), a particular version of which follows:

$$C_{sol} = C_{sol0} F^{D-1}$$

The Rayleigh equation gives the instantaneous concentration of an oxide or element in a solid as a function of C_{sol0}, the initial concentration of that oxide or element in the solid; D, the solid/liquid distribution coefficient; and F, the weight fraction of liquid remaining. Measured zoning profiles give C_{sol} as a function of R, the radius of the grain modeled, but the Rayleigh equation gives C_{sol} as a function of F. An equation relating F and R is derived.

Consider cooling a system comprising the liquid from the isothermal run; call this system the charge (even though it is not the entire charge, but only its liquid fraction at T = 1400°C and log f_{O_2} = IW−3.0). Let ϕ denote the volume fraction of a phase, v denote its volume, ρ denote its density, and w denote its mass fraction. (Of course, $w_{liquid} = F$.) Suppose that olivine and liquid are the only two phases in this system. Then $F = 1 - w_{ol}$. By definition, $w_{ol} = m_{ol}/m_{charge}$. These masses can be expressed in terms of densities and volumes: $w_{ol} = (\rho_{ol} v_{ol})/(\rho_{charge} v_{charge})$, or:

$$w_{ol} = (\rho_{ol} \phi_{ol})/\rho_{charge} \tag{1}$$

ϕ_{ol}, intuitively, should be a function of R: assume all grains have the same R at some F; when R is small, olivine grains are small and ϕ_{ol} must be small, and when R is large, olivine grains are large and ϕ_{ol} must be large. By definition, $\phi_{ol} = v_{ol}/v_{charge}$. Let v_{olf} denote the volume of olivine at some convenient final point (for example, at a quench temperature); multiplying and dividing by v_{olf} gives:

$$\phi_{ol} = (v_{ol}/v_{olf})(v_{olf}/v_{charge}) \tag{2}$$

The second term is just ϕ_{olf}. Assume olivine crystallizes as a spherical shell around relict grains from the isothermal run, giving:

$$v_{ol} = \frac{4}{3}\pi(R^3 - R_{min}^3) \tag{3}$$

R_{min} in (3) is the radius of the relict grain. Suppose R_{max} is the radius of the olivine grain at the final point (e.g., at the quench temperature) considered above; then

$$v_{olf} = \frac{4}{3}\pi(R_{max}^3 - R_{min}^3) \tag{4}$$

Substituting (3) and (4) into (2) and canceling the $\frac{4}{3}\pi$ terms gives:

$$\phi_{ol} = \phi_{olf}(R^3 - R_{min}^3)/(R_{max}^3 - R_{min}^3) \tag{5}$$

In the case where olivine grains start crystallizing from scratch, not around a relict grain, $R_{min} = 0$ and $\phi_{ol} = \phi_{olf}(R/R_{max})^3$. (Note that the cancellation above relaxes the constraint of sphericity: these volume equations apply to olivine crystals that are cubes, parallelpipeds, or even hexagonal prisms as long as R is properly defined.)

Finally, substituting (5) into (1) gives w_{ol} (and therefore F) as a function of R:

$$F(R) = 1 - \frac{\rho_{ol}\phi_{olf}}{\rho_{charge}}\left(\frac{R^3 - R_{min}^3}{R_{max}^3 - R_{min}^3}\right)$$

This can be rearranged to give:

$$F(R) = -\frac{\rho_{ol}\phi_{olf}}{\rho_{charge}(R_{max}^3 - R_{min}^3)}R^3 + \frac{\rho_{ol}\phi_{olf}}{\rho_{charge}(R_{max}^3 - R_{min}^3)}R_{min}^3 + 1$$

This is the useful form $F(R) = aR^3 + k$ where:

$$a = -\frac{\rho_{ol}\phi_{olf}}{\rho_{charge}(R_{max}^3 - R_{min}^3)} \tag{6}$$

$$k = \frac{\rho_{ol}\phi_{olf}}{\rho_{charge}(R_{max}^3 - R_{min}^3)}R_{min}^3 + 1 \tag{7}$$

Now C_{sol} can be found as a function of R:

$$C_{sol} = C_0 D(aR^3 + k)^{D-1}$$

C_{sol0}, the initial concentration of an oxide or element in the solid, can be measured from the crystal core. D, the solid/liquid distribution coefficient, can be calculated for olivine from the measured compositions of the isothermal glass and olivine crystals; published values can also be used (Kennedy et al. 1993). a and k are not so simple: they depend on five values, ρ_{ol}, ϕ_{olf}, ρ_{charge}, R_{max}, and R_{min}, none of which is known precisely. However, while C_{sol0} and D vary between oxides, a and k should be the same for all fractionated oxides or elements in a given olivine crystal. Therefore, the measured zoning profile of an element which has a concentration that depends only upon fractional crystallization (for example, Ca in olivine) can be used to determine the best-fit a and k, which can then be reused with a different C_{sol0} and D to calculate zoning profiles for other elements (Cr or Fe in olivine).

First, modeling is used to verify that fractional crystallization of a liquid that is in equilibrium with Fa_9 crystal cores, hereafter referred to as the starting liquid, cannot explain the fayalite range observed in the cooling runs held at log f_{O_2} = IW$-$0.5. Only Fe profiles of grains with constant-Fa, approximately 20-micron-wide crystal cores are modeled. These constant-Fa cores are probably relict grains from the isothermal runs, since the olivine grains in the isothermal run 10-1 are also 20 microns wide on average and have constant Fa. All large grains of olivine probably crystallized around cores that

formed during the isothermal run; therefore, profiles of large grains without constant-Fa cores (Figure 10) are probably not central sections (i.e., there is no point along the profile where $R = 0$) and cannot be properly modeled with this method.

The method used for modeling the zoning profiles of these grains is as follows: first, the traverse is divided into a core and two rims. For the cooling runs at IW-0.5, a core is the set of all analyzed points less than 1.5 weight percent Fe above the minimum weight percent Fe measured along the traverse. This value of 1.5 weight percent is chosen empirically to give core sizes similar to olivine grains from the isothermal run 10-1. The rims are the set of all other analyzed points. For example, the minimum Fe measured in a CR5 olivine grain is 7.6 weight percent, so the core is the set of all analyzed points with less than 9.1 weight percent Fe and the rim is the set of all analyzed points with a weight percent Fe greater than or equal to 9.1. No crystal cores observed in the cooling runs have a constant concentration of Fe: core inhomogeneity must be attributed to increasing liquid FeO concentration during the soak, since Fe-Mg interdiffusion at the temperatures and oxygen fugacities of the cooling runs is only about 1 micron/hour (Dohmen and Chakraborty 2007).

Next, distances measured along the traverse are transformed into distances (radii) from the center of the crystal core by taking the absolute value of the difference of the distance of an analyzed point from the start of the traverse and the distance of the center of the core from the start of the traverse. (The center of the core is defined as its midpoint: i.e., the point along a traverse equidistant from both edges of the core.) For example, the center of the core of the CR5 olivine grain mentioned above is 39 microns from the start of the traverse; a point 30 microns along the traverse has a radius of $|30 - 39| = 9$ microns. The transformation from distance along traverse to radius folds both halves of the core and both rims around the center of the crystal core.

Next, the core data is discarded; only the rim analyses are used for modeling. The C_{sol0} used for modeling is not the core minimum, but the average of the values at the core edges (cores are inhomogeneous; the very edge of the core best reflects the composition of the starting liquid). Next, a and k are calculated from Ca profiles using nonlinear regression with $D_{measured}$ from Table 10. (Notably, $D_{measured}$ and $D_{published}$ are very similar for Ca and Fe. $D_{measured}$ and $D_{published}$ differ by 0.18 for Cr; Kennedy et al. report a range of 0.6-1.5 for this distribution coefficient at similar conditions in the literature.) a and k are then used to calculate profiles for Cr, another minor element in olivine which has a concentration that is only affected by fractional crystallization, as a check to ensure that these a and k values are reasonable. Finally, a and k are used to calculate profiles for Fe. The folded profiles for each modeled crystal (i.e., profiles with radius, not distance along traverse, on the x-axis), the three calculated profiles, and the calculated a and k are shown in Figure 14 (CR4) and 15 (CR5). The two modeled olivines are the only cooling run olivines with constant-Fa cores (Figure 11).

Element	$D_{measured}$	$D_{published}$
Ca	0.03	0.03
Cr	0.7	0.52
Fe	0.8	0.84

Table 10: Distribution coefficients measured from glass and olivine crystals in the isothermal runs compared to published distribution coefficients at 1200°C with 100°C/hour cooling at log f_{O_2} = IW−0.5 (Kennedy et al. 1993).

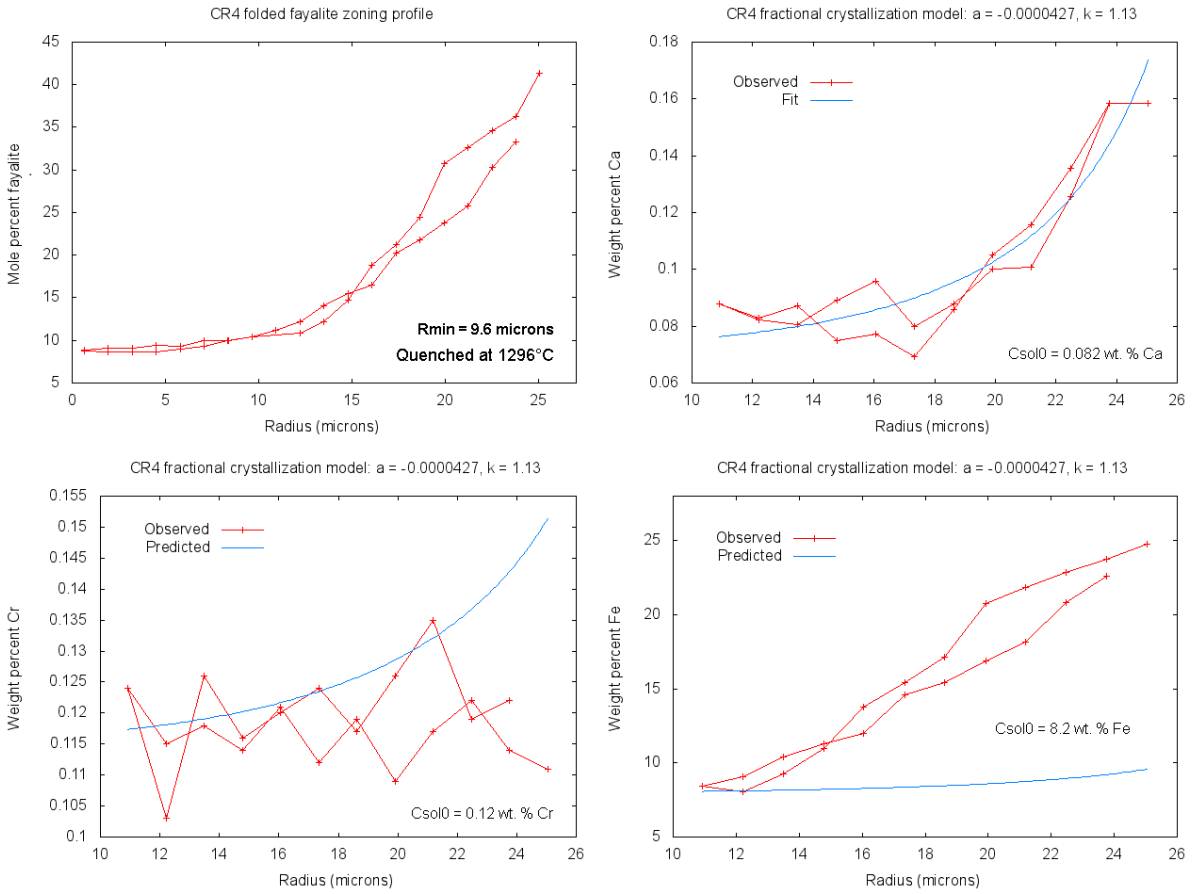

Figure 14: Fractional crystallization model fit to the Ca profile from a CR4 olivine grain and applied to predict Cr and Fe in that grain. 1σ Ca = 0.01 weight percent, 1σ Cr = 0.02 weight percent, and 1σ Fe = 0.1 weight percent (Appendix B).

In the CR4 olivine, the a and k fit to the Ca profile appear to predict one rim of the Cr profile (using an appropriate C_{sol0} and D) . Actually, all concentrations of Cr measured in this grain are the same at the 2σ level; any Cr zoning is buried by analytical error. The Cr fit observed in the CR5 olivine is also bad; again, all measured Cr concentrations are the same at the 2σ level (Appendix B). The predicted CR4 Fe profile falls 15 weight percent short of the measured Fe at the crystal edge; the predicted CR5 profile falls 10 weight percent short of the measured Fe at the crystal edge, evidencing once again that fractional crystallization of the starting liquid cannot produce the Fe zoning profiles observed. Since the CR5 grain has a lower rim edge concentration of Fe than the CR4

grain (21 weight percent Fe vs. 29 weight percent Fe), the CR5 grain must have stopped crystallizing (maybe because it ran up against other crystals) before the liquid reached the FeO concentrations recorded in the CR4 grain. This starting liquid is somewhat richer in Fe (as FeO) than the glass in 10-1 (Table 6): a D of 0.8 and a C_{sol0} of 8.2 weight percent Fe from the core of the CR4 olivine grain give an initial liquid concentration of 13.2 weight percent FeO, a little over four times as high as 3.13, the average weight percent FeO of glass from 10-1. This discrepancy must be explained by the relatively short soak time of CR4 (15 hours soak compared to 23.75 hours soak for 10-1). CR4 has a lower-Fa core than CR5: the minimum concentration measured in the CR4 core is about 6.5 weight percent Fe, whereas the minimum concentration measured in the CR5 core is about 7.6 weight percent Fe; also, the CR4 C_{sol0} is 8.2 weight percent Fe, less than the CR5 C_{sol0} of 9.1 weight percent Fe. The FeO concentration of liquid in the cooling run increases with additional soak time; the CR4 core probably has a lower FeO because it crystallized earlier in the soak than the CR5 core. Finally, values of R_{min} for these grains (9.6 microns and 11 microns for CR4 and CR5 respectively) are similar to the average R_{min} of 11 in the isothermal run 10-1 (Figure 5).

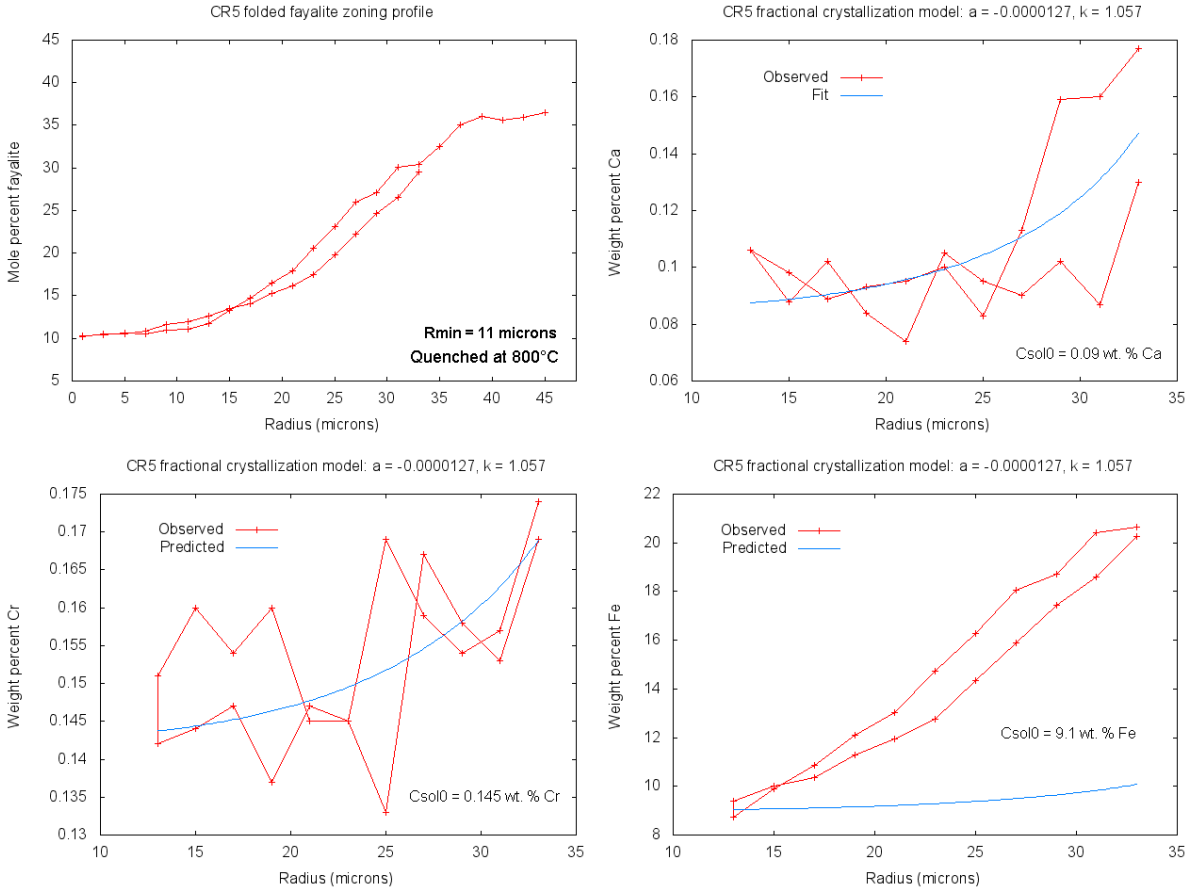

Figure 15: Fractional crystallization model fit to the Ca profile from a CR5 olivine grain and applied to predict Cr and Fe in that grain. 1σ Ca = 0.01 weight percent, 1σ Cr = 0.02 weight percent, and 1σ Fe = 0.1 weight percent (Appendix B).

This application of modeling of fractional crystallization also shows that a and k derived from nonlinear regression of Ca profiles correspond to physical reality. First, for both olivine grains modeled, k has the correct magnitude. When R is 0, F must equal 1, and $F = k$. Both values of k are very close to 1. Second, the values of a and k determined from nonlinear regression of Ca profiles correspond closely to values of a and k calculated from equations (6) and (7). In CR4, olivine is assumed to have an average mole percent fayalite of 20, so ρ_{ol} = 3.4 g/cm^3; an average of olivine and glass density weighted by volume gives ρ_{charge} = 3.1 g/cm^3 for CR4; the core criterion sets R_{min} = 9.6 microns for CR4; the CR4 grain modeled has R_{max} = 25.05 microns; and the starting liquid becomes roughly half olivine by the time CR4 is quenched: ϕ_{olf} = 0.5. (Nonlinear regression was used to determine a and k because of the obvious uncertainties in several of these quantities.) Equations (6) and (7) give a = -0.0000370 and k = 1.033 for CR4, within 20 percent of the the values a = -0.0000427 and k = 1.13 determined from nonlinear regression of the CR4 Ca profile. ρ_{ol} and ρ_{charge} are assumed to remain the same in CR5; however, R_{min}, R_{max} and ϕ_{olf} increase to 11 microns, 33 microns and 0.7 respectively in this run, giving a = -0.0000222 and k = 1.029, within about 50 percent of the values a= -.0000127 and k = 1.057 determined by nonlinear regression of the CR5 Ca profile. The agreement is not great, but there are large uncertainties in the important terms ρ_{ol} and ρ_{charge}. Notably, the absolute values of the calculated a and k and the regressed a and k both decrease from CR4 to CR5. Third and finally, crystal concentrations that correspond to the same melt fraction should have similar concentrations, since the cooling run liquid is nearly homogeneous. The CR4 grain has a concentration of 20 weight percent Fe 21.5 microns from the core (averaging the two rim concentrations); the equation $F(R) = aR^3 + k$ (using regressed a and k) gives F = 0.706; the CR5 grain has a concentration of 20 weight percent Fe 32.5 microns from the core, giving F = 0.621. These two F differ by only 0.08; they should not be exactly the same, since the C_{sol0} of Fe is not the same in CR4 and CR5. In summary, modeling of fractional crystallization based on a and k derived from nonlinear regression of Ca profiles is internally consistent.

Next, an olivine grain from CR11 is modeled. The crystal core of CR11 is defined as the set of all analyzed points less than 0.15 weight percent Fe above the minimum 2.35 weight percent Fe measured along the traverse. This value of 0.15 weight percent Fe is chosen since it is about 1.5σ. The rims are the set of all other analyzed points. The rest of the modeling is the same as for Figures 14 and 15. CR11 was cooled at IW$-$3.0; its Fe profile should show only the effects of fractional crystallization. Figure 16 shows that the Fe profile calculated for CR11 is a much better fit than those calculated for olivine grains in the cooling runs at IW$-$0.5; its Fe still falls somewhat short near the edge, but much less than in the oxidized cooling runs: the departure is 5% of the total average rim Fe, as opposed to about 35% of the total average rim Fe in the cooling runs at IW$-$0.5. This departure is probably due to a poor Ca fit caused by analytical error, since all Ca concentrations in this grain except the highest two measurements are the same at the 2σ level (Appendix B). The departure may be real, however, since the isothermal runs are not at equilibrium and have been shown to lose iron metal (Table 5) with additional time at IW$-$3.0.

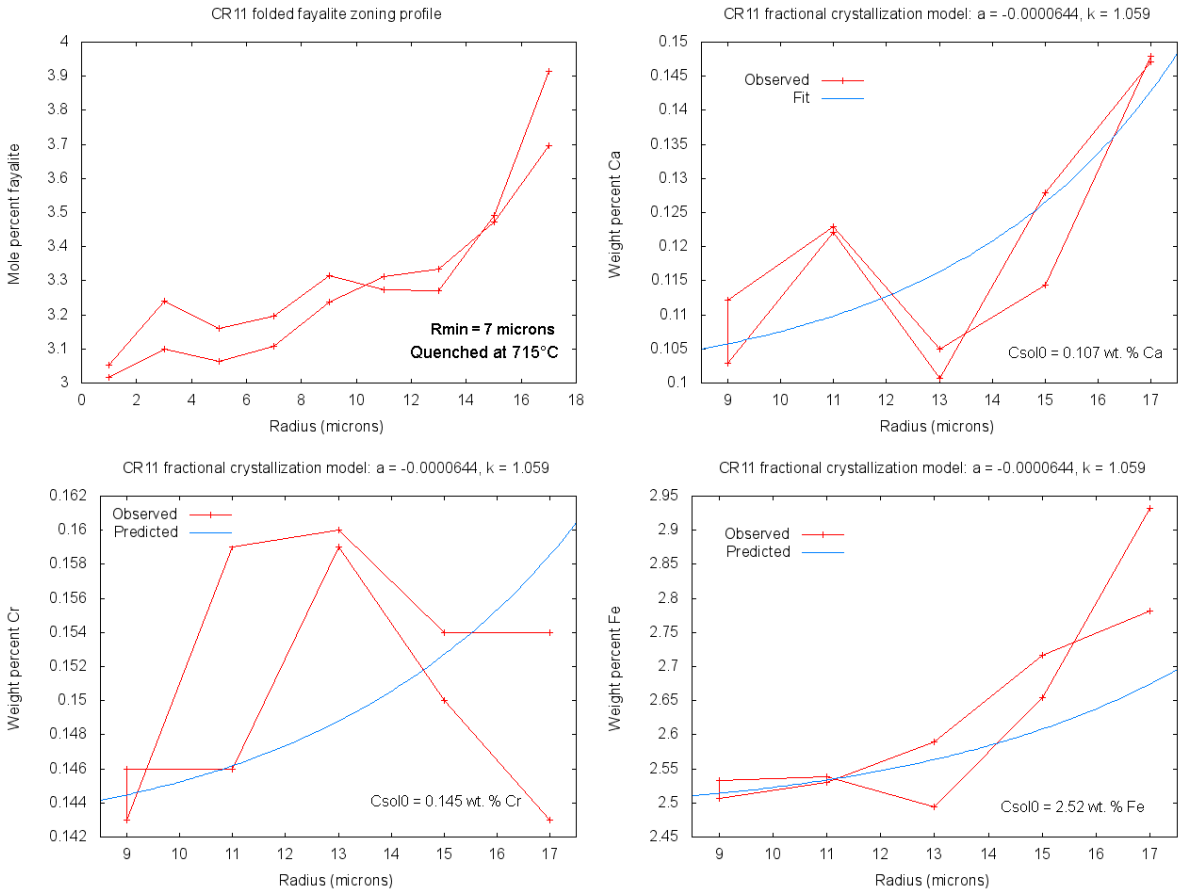

Figure 16: Fractional crystallization model fit to the Ca profile from a CR11 olivine grain and applied to predict Cr and Fe in that grain. 1σ Ca = 0.01 weight percent, 1σ Cr = 0.02 weight percent, and 1σ Fe = 0.1 weight percent (Appendix B).

The Rayleigh equation assumes a closed system: i.e., C_{sol0} is constant. In the cooling runs, however, oxidation of metallic iron increases FeO in the liquid, so C_{sol0} is a non-constant function of F (and therefore R). The most interesting feature of this function is its rate of change. Suppose C_{sol0} is a linear function of R; then the derivative of C_{sol0} is constant–that is, FeO is increasing in the liquid at a constant rate (for low concentrations of FeO, this implies that oxidation is taking place at a constant rate). Suppose, however, that C_{sol0} is proportional to the logarithm of R: then the derivative of C_{sol0} is proportional to $1/R$–oxidation starts fast and then slows to a crawl. Glass FeO spikes between the isothermal run 10-1 and CR4 (Figure 9), cooled for one hour, and then steadily decreases: this suggests oxidation proceeds at some initial, not necessarily constant, fast rate and then proceeds at a slower rate sometime after one hour. It is not clear a priori whether this initial fast rate and changing C_{sol0} is best described as a linear or a logarithmic function of R. (Of course, C_{sol0} is not likely to be exactly a linear or logarithmic function of R; however, knowing which function is a better fit to C_{sol0} gives information about how the rate of oxidation changes.)

In order to determine whether the initial fast rate of oxidation is more nearly a linear or logarithmic function of R, the CR4 grain modeled in Figure 14 is modeled in Figure 17 with C_{sol0} varying as R and as $ln(R)$. a, k, and the initial C_{sol0} are the same as in Figure 14. In the linear model, C_{sol0} is assumed to equal the initial C_{sol0} multiplied by bR, where b is a proportionality constant determined by nonlinear regression. In the logarithmic model, C_{sol0} is assumed to equal the initial C_{sol0} multiplied by $b\ ln(R)$, where b is a proportionality constant determined by nonlinear regression.

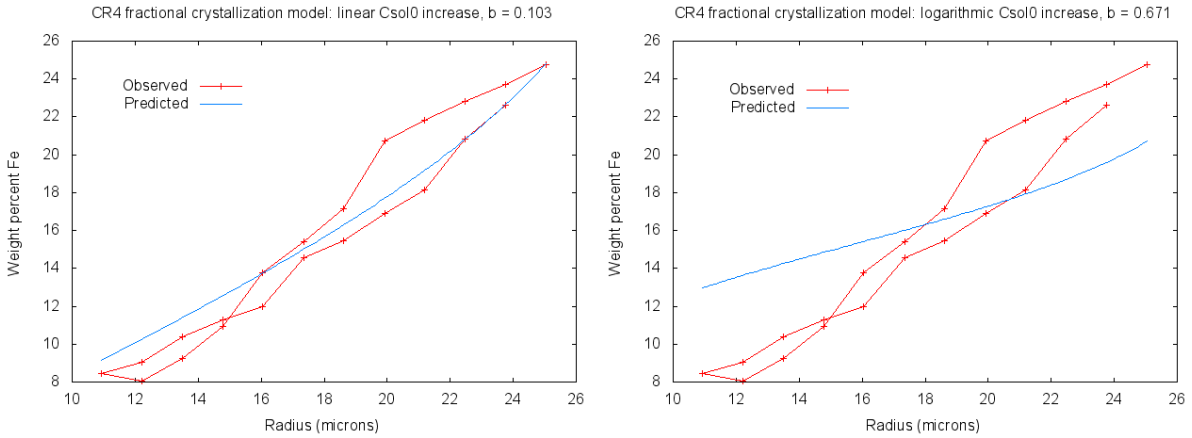

Figure 17: Linear and logarithmic models for C_{sol0} as a function of R applied to predict Fe in a CR4 olivine grain. a, k, and initial C_{sol0} are the same as in Figure 14. 1σ Fe = 0.1 weight percent (Appendix B).

The linear model slightly overestimates the concentration of Fe towards the core of the grain but otherwise closely matches the observed Fe concentration (Figure 17). The logarithmic model overestimates the concentration of Fe towards the core of the grain by up to 5 weight percent and underestimates the concentration towards the edge of the grain by up to 4 weight percent. The linear model gives a much better fit than the logarithmic model, so the rate of oxidation is more nearly proportional to 1 than to $1/R$: at least for the first hour, oxidation progresses at a nearly constant rate. This constant rate cannot continue: no olivine grains from runs cooled longer than 1 hour have Fa contents substantially higher than CR4 (Figure 8); the highest is a grain from CR1 (cooled for four hours) with $Fa_{53.9}$. The absence of grains with Fa contents higher than CR4 olivines cannot be entirely due to slowing crystallization failing to record high liquid FeO, since the FeO of the cooling run glass drops after CR4 (Figure 9). The rate of oxidation might slow soon after CR4 simply because most metallic iron has already been oxidized: the modal abundance of metallic iron is 1.9 percent volume in CR7 (Table 7), which was cooled for three hours, versus about 14 percent volume in the isothermal run 10-1 (Table 5).

Now that the rate and timescale of oxidation have been constrained, what is the extent of the oxidation of metallic iron? In Figure 18, multiple Fe profiles calculated with the a and k from Figures 14 and 15 are plotted across the observed Fe profiles of the CR4 and CR5 grains. These calculated profiles have different values of C_{sol0} chosen to meet measured Fe concentrations. (In Figure 17, a single profile is plotted with a varying

C_{sol0}; in Figure 18, multiple profiles are plotted, each with constant C_{sol0}.) Each calculated profile is a level curve along which Fe concentrations in olivine would evolve if only affected by fractional crystallization. Where the measured profile moves between level curves, FeO is being added to the liquid due to oxidation of metallic iron, effectively increasing the starting C_{sol0}; where the profile moves along level curves, no FeO is being added to the liquid due to oxidation of metallic iron. In the CR4 olivine grain, the C_{sol0} of Fe rises steadily and levels off towards the edge of the grain to meet four datapoints in a row with a C_{sol0} equal to 21.2 weight percent Fe. This weight percent Fe corresponds to 34 weight percent FeO in the CR4 liquid, just below the 35.4 weight percent FeO observed in CR4 glass. The initial steady rise corresponds to the constant change in C_{sol0} observed in Figure 17; the late leveling-off corresponds to the slowing of oxidation when most metallic iron has been oxidized. The CR5 profile rises steadily and never levels off: CR5 stopped crystallizing while oxidation was still taking place at a fast, constant rate. Combining the information about the timescale of oxidation from Figure 17 and the information about the FeO of the liquid from the CR4 profile in Figure 18, it seems that metallic iron oxidizes at a fast, nearly constant rate during most of the first hour of cooling at IW−0.5, raising the FeO concentration of the liquid to about 36 weight percent.

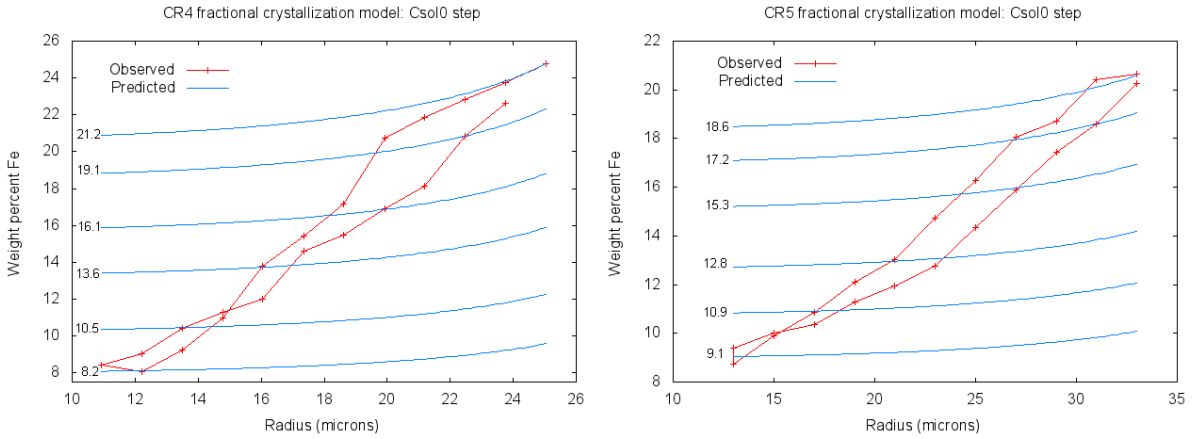

Figure 18: Models stepping C_{sol0} to predict Fe in CR4 and CR5 olivine grains. Predicted curves are labeled with their corresponding C_{sol0} (weight percent Fe). 1σ Fe = 0.1 weight percent (Appendix B).

In summary, modeling of fractional crystallization shows that 1) fractional crystallization of the starting liquid is inadequate to explain the Fa range observed in the cooling runs at IW−0.5; 2) oxidation proceeds at a fast constant rate in the first hour at IW−0.5 and later slows down, probably because most metallic iron has already been oxidized; 3) enough metallic iron is oxidized to produce a maximum of about 37 weight percent FeO in the liquid by the end of the first hour at IW−0.5.

5 Conclusions

Olivines from chondrule composition melts cooled at 100°C/hour while exposed to a gas with log f_{O_2} = IW−0.5 have zoning profiles with a range of over 35 mole percent fayalite (Fa_9 cores to Fa_{45} rims). This fayalite range cannot be produced by fractional crystallization of the starting liquid, a liquid that is in equilibrium with Fa_9 crystal cores: a run cooled at 100°C/hour at log f_{O_2} = IW−3.0 shows a fayalite range of less than 1 mole percent fayalite and modeling of fractional crystallization of the starting liquid predicts a much lower fayalite range than observed. Oxidation of metallic iron in the cooling runs held at IW−0.5 (evidenced by a decrease in modal abundance of metallic iron, a change in shape of metallic iron blebs, and an increase in nickel concentration from the isothermal runs to the cooling runs) adds FeO to the liquid in the cooling runs; fractional crystallization acts on this starting liquid to produce the fayalite range observed.

Modeling of Fe profiles in olivine grains puts constraints on the timescale and extent of oxidation: oxidation starts at a fast constant rate and slows down after the first hour at IW−0.5, probably because most metallic iron has already been oxidized. Enough metallic iron is oxidized to produce about 36 weight percent FeO in the liquid by the end of the shortest cooling run, a twelvefold increase from the weight percent FeO in the isothermal run 10-1. Finally, modeling of Fe profiles could be usefully applied to natural samples–to explain the oxidation history of olivine in Semarkona chondrules, for instance–although it should be kept in mind that the timescale of oxidation from these experiments does not directly apply to solar nebula samples, since the partial pressure of reducing gas in these experiments is probably three orders of magnitude higher than in the solar nebula.

A Appendices

A.1 Rayleigh fractionation and two derivations of the Rayleigh equation

Suppose a substance undergoes a phase transition and that the phase produced is immediately isolated from the original phase of that substance, so that the original phase is, at any time during the phase transition, at equilibrium only with an infinitesimal amount of the phase produced. If some compound in that substance is preferentially partitioned into a particular phase, this process will produce a compositional change in both phases. For example, suppose a compound is perfectly incompatible with the phase produced by the phase transition: if the initial concentration of of the compound in the substance is C_0, the concentration when half that substance remains will be $2C_0$, when one-fourth remains, $4C_0$, when one-eighth remains, $8C_0$, and so on, until the incompatible compound is all that remains in the original phase. This process of chemical evolution by phase transition is called Rayleigh fractionation. Distillation of alcohol, partial melting of the mantle, and fractional crystallization are all examples of Rayleigh fractionation.

Rayleigh fractionation is described quantitatively by the Rayleigh equation. The following derivation is adapted from Albarède (2009). Let m denote the mass of the fractionated compound, M denote the mass of the system, and D denote the solid/liquid distribution coefficient. (The Rayleigh equation is used in this thesis to describe fractional crystallization, so the two phases chosen are solid and liquid; they can be replaced with any other two phases without issue.) The masses of the fractionated compound and the system are partitioned between two phases: $m = m_{liq} + m_{sol}$ and $M = M_{liq} + M_{sol}$. Assuming m and M are constant, differentiating these equations gives two mass balance equations:

$$dm_{liq} + dm_{sol} = 0 \tag{8}$$

$$dM_{liq} + dM_{sol} = 0 \tag{9}$$

An infinitesimal amount of solid is in equilibrium with all the remaining liquid:

$$\frac{dm_{sol}}{dM_{sol}} = D\frac{m_{liq}}{M_{liq}} \tag{10}$$

The mass balance equations (8) and (9) combined with (10) give:

$$\frac{dm_{liq}}{dM_{liq}} = D\frac{m_{liq}}{M_{liq}} \tag{11}$$

This differential equation can be solved for the the mass of the fractionated compound in the liquid, m_{liq}, as a function of the mass of the liquid, M_{liq}. However, it is more useful to change variables to concentration, $C_{liq} = m_{liq}/M_{liq}$, and weight fraction of remaining liquid, $F = M_{liq}/M$, which do not explicitly depend on m_{liq} or M_{liq}.

Differentiating $C_{liq} = m_{liq}/M_{liq}$, dividing by dM_{liq}, and multiplying through by M_{liq} gives:

$$\frac{dm_{liq}}{dM_{liq}} = C_{liq} + M_{liq}\frac{dC_{liq}}{dM_{liq}} \tag{12}$$

Combining (11) and (12) and simplifying gives:

$$\frac{dC_{liq}}{dM_{liq}} = (D-1)\frac{C_{liq}}{M_{liq}} \tag{13}$$

Finally, dividing (13) through by M and noting that $dF = dM_{liq}$ gives a differential equation in terms of C_{liq} and F:

$$\frac{dC_{liq}}{dF} = (D-1)\frac{C_{liq}}{F} \tag{14}$$

The solution of (14) is the Rayleigh equation:

$$C_{liq} = C_0 F^{D-1}$$

C_0 is the initial concentration of the fractionated compound in the liquid. Multiplying through by the distribution coefficient D gives the instantaneous concentration of m in the solid C_{sol} as a function of F:

$$C_{sol} = C_0 D F^{D-1}$$

The form used in this thesis replaces $C_0 D$ with C_{sol0}, the initial instantaneous concentration of the fractionated compound in the solid:

$$C_{sol} = C_{sol0} F^{D-1}$$

A second derivation uses differentials. Consider the system immediately after the phase transition begins, when F is very nearly 1 and an infinitesimal amount of liquid has been transformed to solid. The mass of the fractionated element in the entire system must be equal to the mass of the element in the liquid plus the mass of the element in the solid. Notice that $M = M_{liq}$.

$$CM_{liq} = (C_{liq} - dC_{liq})(M_{liq} - dM_{liq}) + DC_{liq}dM_{liq}$$

Upon simplification, the $dC_{liq}dM_{liq}$ term vanishes; dividing by M to change variables to F gives (14) once again.

A.2 Derivation and calculation of uncertainties in concentrations measured by electron microprobe

In this appendix, an expression for the uncertainties of concentrations measured by electron microprobe is developed and the uncertainties of measured Ca, Cr, and Fe concentrations are calculated.

The x-ray counts produced by a sample bombarded by an electron beam follow a Poisson distribution; therefore, the standard deviation σ of a number of x-ray counts is equal to $\sqrt{n}$, where n is the number of x-ray counts. A concentration measured by electron microprobe is a function of four separate sets of x-ray counts–$n_{p_{sp}}$, the peak counts measured on a specimen; $n_{p_{std}}$, the peak counts measured on a standard; n_{bsp}, the background counts measured on a specimen; and n_{bstd}, the background counts measured on a standard–as well as four count times T corresponding to each set of counts. For most of the Ca and Fe concentrations measured in this thesis, the four count times are equal: $T_{p_{sp}} = T_{p_{std}} = T_{bsp} = T_{bstd}$. For simplicity it is assumed that this is the case for all Ca, Cr, and Fe concentrations measured; for Cr, where the sample and standard count times are different, the shorter count time is used to place an upper bound on the uncertainty. The X-ray intensity I is defined as n/T, the ratio of the number of counts to the count time.

The K-ratio of an element for a given analysis, $K = (I_{p_{sp}} - I_{bsp})/(I_{p_{std}} - I_{bstd})$, is approximately equal to the ratio of the concentration of the element in that analysis to its concentration in the standard. The expression for the standard deviation of n, the condition that $T_{p_{sp}} = T_{p_{std}} = T_{bsp} = T_{bstd}$, and the rules for the products and sums of standard deviations give the following equation for the relative uncertainty of the K-ratio, σ_k/K:

$$\sigma_k/K = \sqrt{\frac{1}{T}\left(\frac{I_{p_{sp}} + I_{bsp}}{(I_{p_{sp}} - I_{bsp})^2} + \frac{I_{p_{std}} + I_{bstd}}{(I_{p_{std}} - I_{bstd})^2}\right)}$$

This equation is used to calculate the relative uncertainties in Table 11:

	$I_{p_{sp}}$	I_{bsp}	$I_{p_{std}}$	I_{bstd}	T	σ_k/K
Ca	45	17	3255	19	30	0.051
Cr	95	44	12609	95	20	0.052
Fe	1189	12	1449	14	30	0.007

Table 11: Peak and background intensities (counts/second) and count times (seconds) for Ca, Cr, and Fe measured on standards and on a representative olivine grain from CR1 plus calculated σ_k/K.

The relative uncertainties for Ca and Cr are small: if cooling run olivine has 0.125 weight percent Ca and 0.15 weight percent Cr on average, then 1σ for Ca is a little less than 0.01 weight percent and 1σ for Cr is a little less than 0.02 weight percent. Core to rim variation for Ca profiles is >10σ and core to rim variation for Cr profiles is >5σ: the fits in the Discussion are generally good, but the uncertainties of the measured Ca and Cr concentrations (particularly Cr) must be kept in mind. The relative uncertainty

of Fe is very small : if cooling run olivine has a concentration of 15 weight percent Fe on average, 1σ for Fe is about 0.1 weight percent. Core to rim variation for Fe profiles is >100σ. Finally, CR5 and CR11 Ca and Fe analyses have shorter sample and standard count times (20 seconds standard count time/15 seconds sample count time for Ca; 30 seconds standard count time/20 seconds sample count time for Fe) than Ca and Fe analyses on other CR samples. The σ_k/K for Ca and Fe in CR5 and CR11 are slightly greater than those reported in Table 11, but the uncertainties of CR5 and CR11 Ca and Fe concentrations are still less than 0.01 and 0.1 weight percent respectively.

References

M. D. Abramoff, P. J. Magelhaes, and S. J. Ram. Image Processing with ImageJ. *Biophotonics International*, 11:36–42, 2004.

F. Albarède. *Geochemistry: An Introduction*. Cambridge University Press, 2nd edition, 2009.

J. R. Beckett. *The origin of calcium-, aluminum-rich inclusions from carbonaceous chondrites: an experimental study*. PhD thesis, University of Chicago, 1986. 373 p.

R. Dohmen and S. Chakraborty. Fe-Mg diffusion in olivine II: point defect chemistry, change of diffusion mechanisms and a model for calculation of diffusion coefficients in natural olivine. *Physics and Chemistry of Minerals*, 34:409–430, 2007.

D. S. Ebel and L. Grossman. Condensation in dust-enriched systems. *Geochimica et Cosmochimica Acta*, 64:339–366, January 2000.

L. Grossman, J. R. Beckett, A. V. Fedkin, S. B. Simon, and F. J. Ciesla. Redox conditions in the solar nebula: Observational, experimental, and theoretical constraints. *Reviews in Mineralogy and Geochemistry*, 68(1):93–140, January 2008.

E. Jarosewich. Chemical analyses of meteorites - a compilation of stony and iron meteorite analyses. *Meteoritics*, 25:323–337, December 1990.

R. H. Jones. Petrology of FeO-poor, porphyritic pyroxene chondrules in the Semarkona chondrite. *Geochimica et Cosmochimica Acta*, 58:5325–5340, December 1994.

A. K. Kennedy, G. E. Lofgren, and G. J. Wasserburg. An experimental study of trace element partitioning between olivine, orthopyroxene and melt in chondrules: equilibrium values and kinetic effects. *Earth and Planetary Science Letters*, 115(1-4):177–195, 1993.

M. R. Lee and P. A. Bland. Mechanisms of weathering of meteorites recovered from hot and cold deserts and the formation of phyllosilicates. *Geochimica et Cosmochimica Acta*, 68(4):893–916, 2004.

S. B. Simon. Chondrule-Composition Melts: Response of Fe and Ti Valence to Changing Redox Conditions. Talk presented at LPSC 42, 2011.

S. B. Simon, J. R. Beckett, W. M. Vaughan, S. R. Sutton, and L. Grossman. Chondrule-Composition Melts: Response of Fe and Ti Valence to Changing Redox Conditions. In *Lunar and Planetary Institute Science Conference Abstracts*, volume 42, Abstract #1271, March 2011.

S. B. Simon, S. R. Sutton, and L. Grossman. The Valence of Titanium in Refractory Forsterite. In *Lunar and Planetary Institute Science Conference Abstracts*, volume 38, Abstract #1892, March 2007.

S. B. Simon, S. R. Sutton, and L. Grossman. Constraints on the Oxidation State of Chondrule Precursors from Titanium XANES Analysis of Semarkona Chondrules. In *Lunar and Planetary Institute Science Conference Abstracts*, volume 39, Abstract #1352, March 2008.

T. Williams and K. Kelley. Gnuplot 4.4: an interactive plotting program. http://gnuplot.sourceforge.net/, March 2010.